










Ventral tegmental area GABAergic inhibition of cholinergic interneurons in the ventral nucleus accumbens shell promotes reward reinforcement

Ream Al-Hasani^{1,2,3,14}  , Raajaram Gowrishankar^{4,5,14}, Gavin P. Schmitz^{1,3,14}, Christian E. Pedersen^{4,5,6}, David J. Marcus^{4,7}, Sofia E. Shirley⁴, Taylor E. Hobbs^{8,9,10} , Abigail J. Elerding⁴, Sophie J. Renaud³, Miao Jing^{7,8,9,10}, Yulong Li^{8,9,10} , Veronica A. Alvarez¹¹ , Julia C. Lemos^{11,12} and Michael R. Bruchas^{3,4,5,6,13}  

The long-range GABAergic input from the ventral tegmental area (VTA) to the nucleus accumbens (NAc) is relatively understudied, and therefore its role in reward processing has remained unknown. In the present study, we show, in both male and female mice, that long-range GABAergic projections from the VTA to the ventral NAc shell, but not to the dorsal NAc shell or NAc core, are engaged in reward and reinforcement behavior. We show that this GABAergic projection exclusively synapses on to cholinergic interneurons (CINs) in the ventral NAc shell, thereby serving a specialized function in modulating reinforced reward behavior through the inhibition of ventral NAc shell CINs. These findings highlight the diversity in the structural and functional topography of VTA GABAergic projections, and their neuromodulatory interactions across the dorsoventral gradient of the NAc shell. They also further our understanding of neuronal circuits that are directly implicated in neuropsychiatric conditions such as depression and addiction.

Neuronal projections from the VTA to the NAc are a crucial component of the brain's reward circuitry, are critical in learning motivationally relevant environmental stimuli^{1–4} and are maladapted in depression and addiction^{5–8}. These functions have largely been ascribed to VTA-to-NAc dopamine (DA)-projecting neurons; however, a growing body of literature has now identified glutamatergic and GABA (γ -aminobutyric acid)-ergic release in the NAc to also play critical roles in reward, salience and aversion behaviors^{9,10}. Whereas glutamate and DA projections from the VTA to the NAc (including DA populations that co-release glutamate and GABA) have received widespread attention, a large subpopulation of inhibitory GABA-releasing neurons also project from the VTA to the NAc^{11–14}, yet how they contribute to motivation, reward and reinforced behavior has not been established. One of the most direct studies exploring the role of VTA^{VGAT}-NAc neurons showed that these terminals selectively inhibit CINs in the NAc and are involved in aversive cue-associative learning¹². The NAc is important for reinforcement learning, and inhibition of NAc CINs has been shown to signal salience and to be involved in the learning of drug–context associations¹⁵.

The aforementioned studies, however, primarily targeted the NAc core (NAcC) and do not account for the vast heterogeneity within the NAc that extends beyond the NAcC and shell (NAcSh) subdivisions¹³.

There has been a growing appreciation for distinct dopaminergic inputs into the core versus the shell, which differentially contribute to reward and aversion¹⁶. Within the NAcSh, there exist subregion-specific NAc subpopulations composed of distinct neural circuits, which contribute differently to reward, aversion and reinforcement to ultimately orchestrate motivated behavior^{17,18}. Perhaps the more widely studied distinction is along the rostrocaudal axis, receiving heterogeneous functional input and contributing to distinct behaviors¹⁹. Importantly for the present study, we previously identified diverse subpopulations across the dorsoventral axis of the NAcSh that promote opposing behaviors (reward versus aversion)¹⁷. Yet, whether and how GABA projection neurons contribute to this functional heterogeneity and interact with key neuromodulator systems in the NAc are unknown. In the present study, we examined the functional role of long-range VTA-NAc GABAergic neurons (VTA^{VGAT}-NAc), and identify a specialized function for these neurons in facilitating reward processing through direct projections to the ventral NAcSh (vNAcSh) CINs but not other NAc subregions (that is, core, dorsal (d)NAcSh).

Results

VTA GABAergic terminals in the vNAcSh are engaged during reward processing. The NAc is a heterogeneous structure in both its anatomical and its cellular composition¹⁸. Functional differences

¹Center for Clinical Pharmacology, University of Health Sciences and Pharmacy and Washington University in St. Louis School of Medicine, St. Louis, MO, USA. ²Department of Pharmaceutical and Administrative Sciences, University of Health Science and Pharmacy, St. Louis, MO, USA. ³Department of Anesthesiology, Washington University in St. Louis, St. Louis, MO, USA. ⁴Center for the Neurobiology of Addiction, Pain and Emotion, University of Washington, Seattle, WA, USA. ⁵Department of Anesthesiology and Pain Medicine, University of Washington, Seattle, WA, USA. ⁶Department of Bioengineering, University of Washington, Seattle, WA, USA. ⁷Chinese Institute for Brain Research, Beijing, China. ⁸State Key Laboratory of Membrane Biology, Peking University School of Life Sciences, Beijing, China. ⁹PKU-IDG/McGovern Institute for Brain Research, Beijing, China. ¹⁰Peking-Tsinghua Center for Life Sciences, Beijing, China. ¹¹Laboratory on Neurobiology of Compulsive Behaviors, Intramural Research Program, National Institute on Alcohol Abuse and Alcoholism, National Institutes of Health, Bethesda, MD, USA. ¹²Department of Neuroscience, University of Minnesota, Minneapolis, MN, USA. ¹³Department of Pharmacology, University of Washington, Seattle, WA, USA. ¹⁴These authors contributed equally: Ream Al-Hasani, Raajaram Gowrishankar, Gavin P. Schmitz.  e-mail: al-hasanir@wustl.edu; mbruchas@uw.edu

along both the rostrocaudal and the dorsoventral axes have been reported regarding aversive and reward-like behavioral states^{17,19–21}, which suggest differential connectivity within this NAcSh subregion. The role of VTA GABA projections into these different NAcSh regions in the modulation of reinforced behaviors is not known. To directly examine the functional role of these VTA^{VGAT}-NAc projections, we expressed the genetically encoded calcium indicator GCaMP6s²² selectively in GABA neurons of the VTA, and implanted an optical fiber in either the vNAcSh or the dNAcSh (as previously determined and described¹⁷) of *VGAT-IRES-cre* mice (Fig. 1a and Extended Data Fig. 1a). After virus expression, we recorded GCaMP activity in VTA^{VGAT}-NAc terminals in either the vNAcSh or the dNAcSh using fiber photometry, while animals underwent either pavlovian conditioning (Fig. 1b,c) or operant conditioning (Extended Data Fig. 1i). On pellet delivery, the animals performed head entries into the pellet receptacle for reward retrieval, followed by pellet consumption. They also performed intertrial interval (ITI) head entries throughout the session, with a significant decrease in ITI head entries across pavlovian conditioning (Extended Data Fig. 1b), indicative of positive reinforcement behavior. There was a significant decrease in the latency for pellet retrieval on day 5 compared with day 1, in both VTA^{VGAT}-vNAcSh and -dNAcSh groups, demonstrating pavlovian conditioning (Fig. 1d). Furthermore, there was increased GCaMP activity during cue presentation and reward delivery, retrieval and consumption (Fig. 1e); however, fluctuations in activity were greater in the VTA^{VGAT}-vNAcSh projection. Specifically, we observed that VTA^{VGAT}-vNAcSh terminals showed a sustained increase in GCaMP activity during cue presentation, in anticipation of a reward that did not change across conditioning (Fig. 1f(top),i–k). We also found much higher peak GCaMP fluorescence after pellet delivery during the period encompassing head entries for reward retrieval and consumption. There was also an increase in strengthening of the peak calcium activity across pavlovian conditioning days, with significantly higher maximal GCaMP fluorescence response on day 5 compared with day 1 (Fig. 1g(top),i–k). Specifically, we observed increased activity in VTA^{VGAT}-vNAcSh terminals during pellet retrieval and consumption (Extended Data Fig. 1c), but not during unrewarded, seeking-like ITI head entries (Extended Data Fig. 1d). In contrast, there was a significant increase in the peak calcium activity for VTA^{VGAT}-dNAcSh projections during cue presentation (Fig. 1f(bottom),l–n) and, unlike VTA^{VGAT}-vNAcSh terminals, no significant increase in fluorescent activity across

training after reward delivery (Fig. 1g(bottom),l–n) was observed. We also found that GCaMP activity to cue persisted during pavlovian extinction in both vNAcSh and dNAcSh groups (Extended Data Fig. 1g,h), bolstering our findings that VTA^{VGAT}-vNAcSh projections are maximally active during reward retrieval and consumption, as opposed to cue presentation. We also report that maximal GCaMP activity during reward consumption was significantly higher in the VTA^{VGAT}-vNAcSh compared with the dNAcSh terminals, whereas peak fluorescence during cue presentation was unchanged (Fig. 1h).

After pavlovian conditioning, animals underwent operant training in both fixed ratio 1 and 3 schedules (FR-1 and -3) (Extended Data Fig. 1i). Both VTA^{VGAT}-vNAcSh and -dNAcSh groups showed a significant increase in active nose pokes for reward on day 3 of FR-1 compared with day 1 (Extended Data Fig. 1j), and reward retrieval and consumption behaviors after pellet delivery. Peak GCaMP fluorescence activities to both cue and reward delivery were sustained in the VTA-vNAcSh^{VGAT} terminals (Extended Data Fig. 1k,l(top) and Extended Data Fig. 1n,o); however, maximal GCaMP fluorescence responses were significantly reduced in the VTA-dNAcSh^{VGAT} projections as animals progressed through operant conditioning (Extended Data Fig. 1k,l(bottom) and Extended Data Fig. 1p,q). This was further apparent when we compared peak fluorescence across VTA-NAcSh^{VGAT} projections during operant conditioning; similar to pavlovian training, we found significantly higher GCaMP activity during reward consumption in the VTA-vNAcSh^{VGAT} compared with the VTA-dNAcSh terminals (Extended Data Fig. 1m).

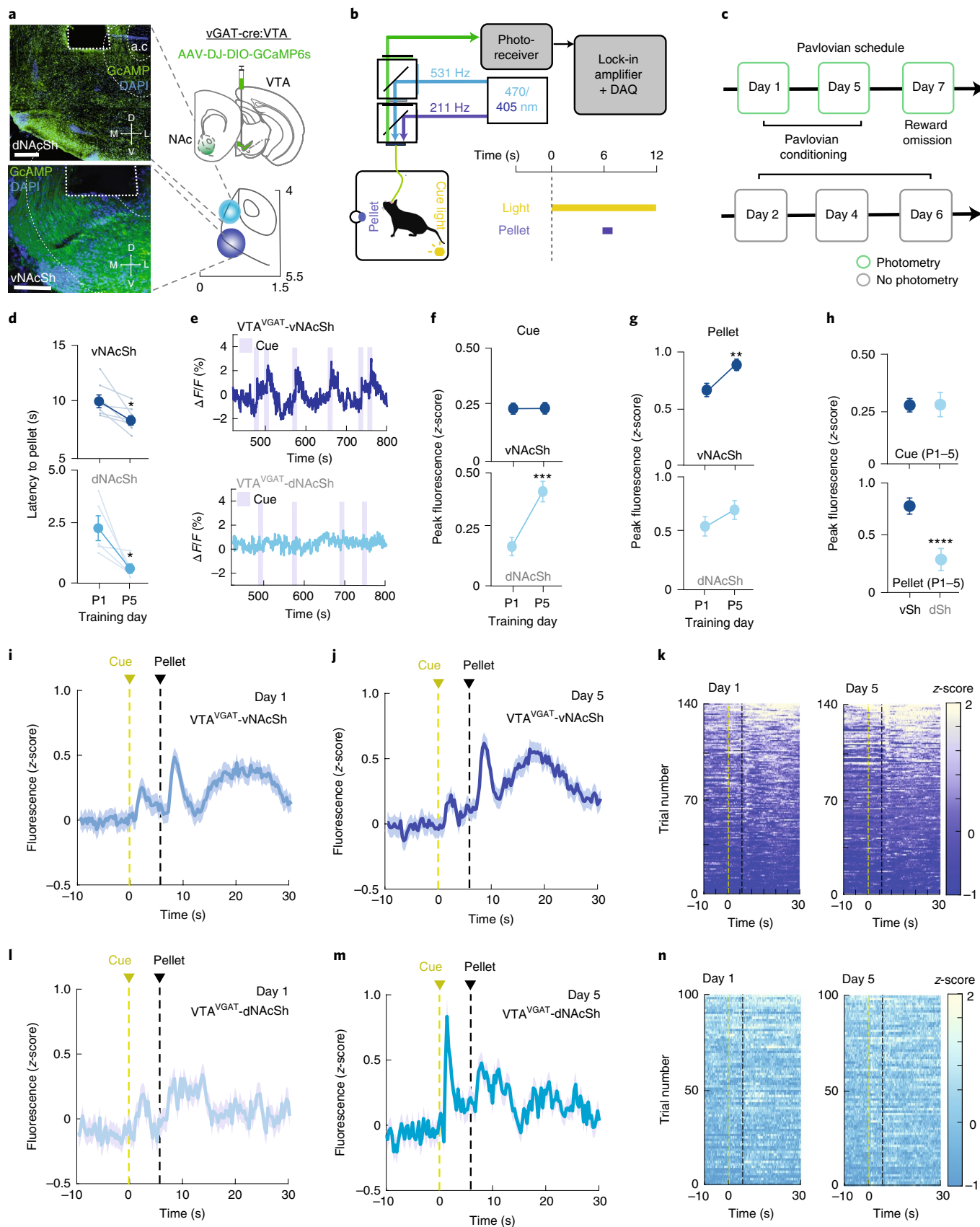
Taken together, these results indicate that long-range VTA-vNAcSh^{VGAT} projections are robustly engaged during reward retrieval and consumption, with only a modest response to associated cues. However, VTA-dNAcSh^{VGAT} terminals are significantly more active during cues that predict an outcome, in accordance with previous studies that ascribe a role for cue discrimination for VTA-NAc^{VGAT} projections^{10,12}.

VTA GABAergic projections to the vNAcSh impacts reward reinforcement. To determine whether direct activation of VTA^{VGAT}-NAc projection is sufficient to modulate reward behaviors, we injected AAV5-DIO-ChR2-eYFP into the VTA of *vGAT-IRES-cre* mice and first determined the effects of photostimulation on this circuit. Optical fibers were implanted into three distinct NAc regions: vNAcSh, dNAcSh or NAAC (Fig. 2a)^{13,15}. The effects of various stimulation parameters were tested in a frequency response curve ranging

Fig. 1 | VTA GABAergic terminals in the vNAcSh are preferentially engaged during reward reinforcement. **a**, Coronal brain schematic of viral injection of GCaMP6s into VTA and fiber expression in the NAc of *VGAT-IRES-Cre*⁺ mice (right, top), and representative spread of expression in the dNAcSh or vNAcSh (right, bottom). Representative x20 coronal image (left panel) showing expression of GCaMP6s (green), DAPI (blue) and fiber placement in dNAcSh (top) and vNAcSh (bottom). Scale, 200 μ m. **b**, Schematic of fiber photometry setup and data acquisition (DAQ) connected to mouse performing a pavlovian task. **c**, Pavlovian training schedule with photometry recordings, as indicated. **d**, Latency to eat after reward delivery (0–6 s) for pavlovian training. Top: vNAcSh ($n = 7$ mice; P1 versus P5, paired Student's t -test, $*P = 0.0163$, $t = 3.308$, degrees of freedom (d.f.) = 6). Bottom: dNAcSh ($n = 5$ mice; P1 versus P5, paired Student's t -test, $*P = 0.0268$, $t = 2.709$, d.f. = 4). Data are represented as mean \pm s.e.m. **e**, Representative recorded GCaMP activity in the vNAcSh (top) or dNAcSh (bottom) during pavlovian training (highlights represent cue light during reward period). **f**, Peak fluorescence during cue period (0–6 s) for pavlovian training. Top: vNAcSh ($n = 7$ mice; P1 versus P5, paired Student's t -test, $***P = 0.8437$, $t = 0.19175$, d.f. = 135). Bottom: dNAcSh ($n = 5$ mice; P1 versus P5, paired Student's t -test, $P < 0.0001$, $t = 4.067$, d.f. = 97). Data represented as mean \pm s.e.m. **g**, Peak fluorescence during reward period (6–30 s) for pavlovian training. Top: vNAcSh ($n = 7$ mice; P1 versus P5, paired Student's t -test, $**P = 0.0031$, $t = 3.016$, d.f. = 135). Bottom: dNAcSh ($n = 5$ mice; P1 versus P5, paired Student's t -test, $P = 0.2438$, $t = 1.175$, d.f. = 97). Data are represented as mean \pm s.e.m. **h**, Top: peak fluorescence during cue period (0–6 s) comparing vNAcSh ($n = 7$ mice) versus dNAcSh ($n = 5$ mice) for pavlovian training (unpaired Student's t -test, $****P = 0.9638$, $t = 0.0454$, d.f. = 680). Bottom: peak fluorescence during reward period (6–30 s) comparing vNAcSh ($n = 7$ mice) versus dNAcSh ($n = 5$ mice) for pavlovian training (unpaired Student's t -test, $P < 0.0001$, $t = 5.106$, d.f. = 682). Data are represented as mean \pm s.e.m. **i**, Mean vNAcSh-recorded calcium activity averaged across all trials from day 1 of pavlovian conditioning ($n = 7$ mice). Data are represented as mean \pm s.e.m. **j**, Mean vNAcSh-recorded calcium activity averaged across all trials from day 5 of pavlovian conditioning ($n = 7$ mice). Data are represented as mean \pm s.e.m. **k**, Heatmap raster plot of vNAcSh-recorded calcium activity for every trial of pavlovian conditioning on day 1 (left) and day 5 (right). Trials are displayed in ascending order by average activity after pellet delivery ($n = 7$ mice). **l**, Mean dNAcSh-recorded calcium activity averaged across all trials from day 1 of pavlovian conditioning ($n = 5$ mice). Data are represented as mean \pm s.e.m. **m**, Mean dNAcSh-recorded calcium activity averaged across all trials from day 5 of pavlovian conditioning ($n = 5$ mice). Data are represented as mean \pm s.e.m. **n**, Heatmap raster plot of dNAcSh-recorded calcium activity for every trial of pavlovian conditioning on day 1 (left) and day 5 (right). Trials are displayed in ascending order by average activity after pellet delivery ($n = 5$ mice).

from 0 Hz to 60 Hz (Extended Data Fig. 2d,j,o). Photostimulation of VTA^{VGAT-vNAcSh} terminals, but not in the dNAcSh or the NAcC, resulted in a significant increase in time spent in the stimulation

side using a real-time place testing paradigm¹⁷ (Fig. 2b,c,d). These results indicate that activation of VTA^{VGAT-vNAcSh} projections can facilitate real-time preference behavior.



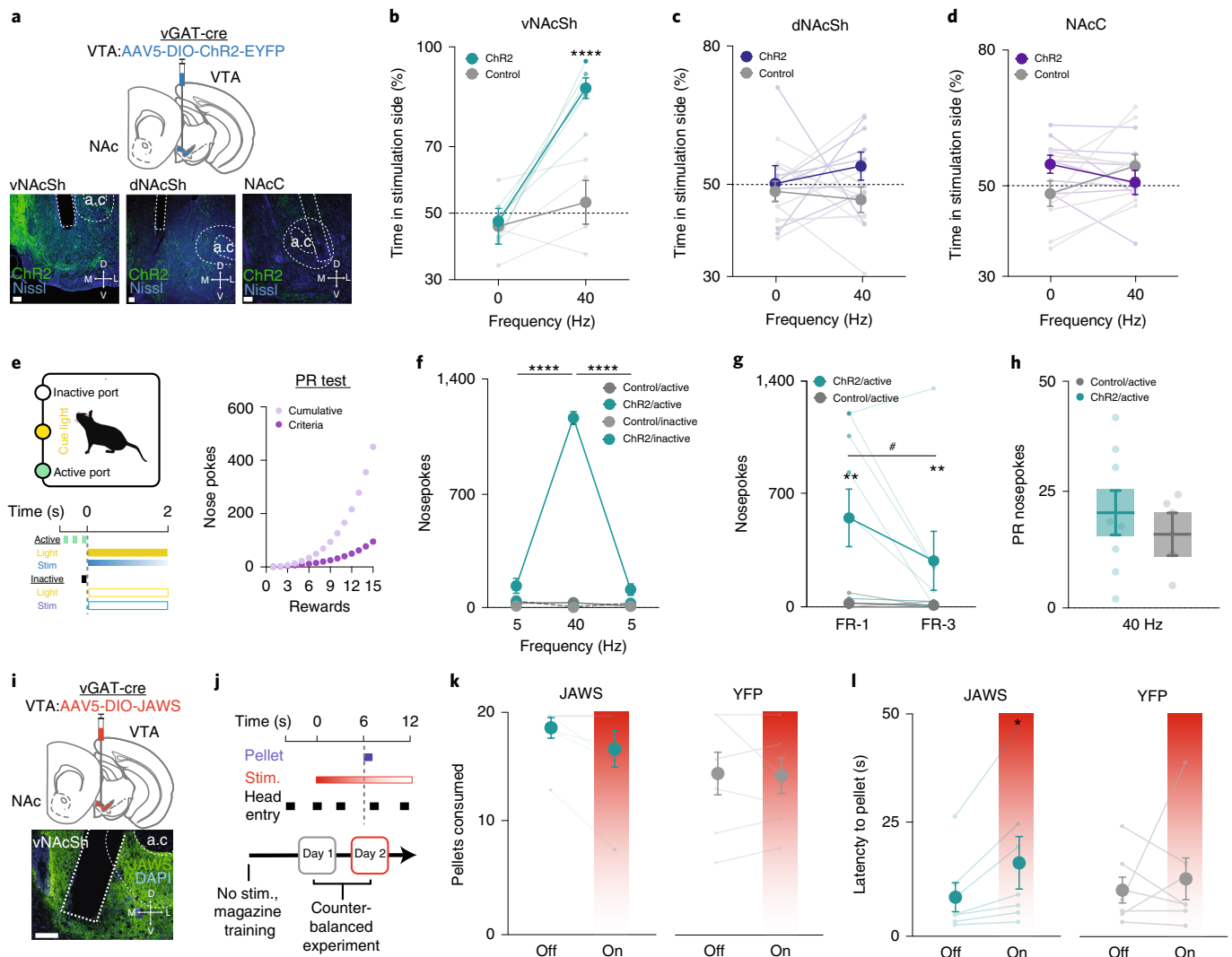


Fig. 2 | Bidirectional photomanipulation of VTA GABAergic projections to the vNAcSh impacts reward reinforcement. **a**, Top: coronal brain cartoon of viral injection of Chr2 into the VTA and fiber expression in the NAc of VGAT-Cre⁺ mice. Bottom: representative $\times 20$ coronal image (left) showing expression of Chr2 (green), Nissl (blue) and fiber placement in vNAcSh (left), dNAcSh (middle) and NAcC (right). Scale, 100 μm . **b**, Photostimulation of vGAT terminal in vNAcSh at 40 Hz, 20-ms pulse width shows a significant preference. Two-way, repeated-measure ANOVA (control versus Chr2: $F[1,8]=15.83$, $P=0.0040$; 0 versus 40 Hz: $F[1,8]=47.48$, $P=0.0001$; interaction: $F[1,8]=22.96$, $P=0.0014$); Bonferroni's post-hoc analysis (control versus Chr2, **** $P < 0.0001$, $t=6.069$, d.f.=16; Chr2 group 0 versus 40 Hz: **** $P < 0.0001$, $t=9.236$, d.f.=8). Data are represented as mean \pm s.e.m. ($n=6$ mice, control; 7 mice, Chr2). **c**, Photostimulation of vGAT terminal in dNAcSh at 40 Hz, 20-ms pulse width. Two-way, repeated-measure ANOVA (control versus Chr2: $F[1,15]=2.840$, $P=0.1126$; 0 versus 40 Hz: $F[1,15]=0.09334$, $P=0.7642$; interaction: $F[1,15]=0.7677$, $P=0.3947$, $n=8$ mice, control; 10 mice, Chr2); Bonferroni's post-hoc analysis (control versus Chr2: $P > 0.9999$, $P=0.4447$, d.f.=15; Chr2 group 0 versus 40 Hz: $P=0.9061$, $t=0.7704$, d.f.=15, $n=10$ mice). Data are represented as mean \pm s.e.m. **d**, Photostimulation of vGAT terminal in NAcC at 40 Hz, 20-ms pulse width. Two-way, repeated-measure ANOVA (control versus Chr2: $F[1,30]=0.3$, $P=0.5773$; 0 versus 40 Hz: $F[1,30]=0.1$, $P=0.6830$; interaction: $F[1,30]=3.9$, $P=0.0550$); Bonferroni's post-hoc analysis (control versus Chr2: $P=0.1606$, $t=1.810$, d.f.=30, $n=8$ mice, control and $n=9$ mice, Chr2; Chr2 group 0 versus 40 Hz: $P=0.6380$, $t=1.013$, d.f.=30, $n=9$ mice). Data are represented as mean \pm s.e.m. **e**, Schematic outlining experimental procedure of operant testing. **f**, Significant differences in active nose pokes in response to 5-Hz photostimulation reward versus 40-Hz photostimulation reward and a 40-Hz photostimulation reward versus 5-Hz photostimulation reward again. Both Chr2 5 Hz versus 40 Hz (unpaired, two-tailed Student's t -test, **** $P < 0.0001$, d.f.=4, $n=5$ mice/5 Hz, 7 mice/40 Hz). Data are represented as mean \pm s.e.m. **g**, Data showing number of nose pokes during FR-1 testing versus FR-3 testing. Control versus Chr2 (unpaired, two-tailed Student's t -test, ** $P=0.0296$, $t=2.694$, d.f.=18, $n=4$ mice for control and 7 mice for Chr2; unpaired, two-tailed Student's t -test); Chr2 FR-1 versus FR-3 (* $P=0.031$, $t=2.974$, d.f.=9, $n=7$ mice). Data are represented as mean \pm s.e.m. **h**, Data showing number of nose pokes during progressive ratio testing with no significant differences between control and experimental groups (unpaired, two-tailed Student's t -test, $P=0.6048$, $t=0.7902$, d.f.=12). Data are represented as mean \pm s.e.m. ($n=6$ mice for control and 8 mice for Cre⁺). **i**, Top: coronal brain cartoon of viral injection of JAWS into VTA and fiber expression in the NAc of VGAT-Cre⁺ mice. Bottom: representative $\times 40$ coronal image (left panel) showing expression of JAWS (green), DAPI (blue) and fiber placement in vNAcSh. Scale, 100 μm . **j**, Cartoon outlining experimental procedure of uncued reward delivery testing. Stim., stimulation. **k**, Total pellets consumed in matched, counterbalanced sessions comparing laser on versus off (pulse 2 s on, 2 s ramp down, 1 s off). Left: JAWS group ($n=7$ mice; off versus on, paired Student's t -test, $P=0.0582$, $t=2.335$, d.f.=6). Right: YFP group ($n=7$ mice; off versus on, paired Student's t -test, $P=0.8461$, $t=0.2027$, d.f.=6). Data are represented as mean \pm s.e.m. **l**, Pellet retrieval latencies in matched, counterbalanced sessions comparing laser on versus off (pulse 2 s on, 2 s ramp down, 1 s off). Left: JAWS group ($n=7$ mice; off versus on, paired Student's t -test, $P=0.0308$, $t=2.810$, d.f.=6). Right: YFP group ($n=7$ mice; off versus on, paired Student's t -test, $P=0.6443$, $t=0.4859$, d.f.=6). Data are represented as mean \pm s.e.m.

To further assess whether activation of the VTA^{VGAT}-vNAcSh projection can also increase reinforcement, we trained mice in a self-stimulation operant paradigm whereby they nosepoke to receive photostimulation (Fig. 2e). Photostimulation of VTA^{VGAT}-vNAcSh terminals resulted in a significant and robust increase in nosepoking for self-stimulation under an FR-1 schedule (Fig. 2f), indicating that activation of these terminals can promote reinforcing behaviors. It is interesting that, whereas mice still performed nosepokes for VTA^{VGAT}-vNAcSh self-stimulation when the schedule was increased to an FR-3 relative to controls, they performed significantly fewer nosepokes compared with FR-1 self-stimulation (Fig. 2g). Moreover, mice made a similar number of nosepokes compared with controls under a PR paradigm for light stimulation (Fig. 2h). These FR-3 and PR findings demonstrate a lack of reinforcement behavior under increased effort, suggesting that VTA^{VGAT}-vNAcSh projections are not likely to be involved in regulating motivation. Thus, taken together these photoactivation results implicate activation of VTA^{VGAT}-vNAcSh projections as sufficient to increase reinforced operant behavior.

Our photometry results suggest that VTA^{VGAT}-vNAcSh terminals are primarily engaged after reward delivery, including positively reinforcing behaviors such as reward seeking (head entries), reward retrieval and reward consumption. We next examined the necessity of VTA^{VGAT}-vNAcSh in the natural reward-associated behaviors, specifically involving reward seeking and retrieval, by inhibiting VTA^{VGAT}-vNAcSh terminals using the red-shifted chloride pump JAWS (using stimulation parameters previously determined and described²³) during a simple, noncued reward task assaying pellet consumption and reward-seeking head entry events. We injected AAV5-DIO-JAWS-YFP into the VTA and implanted bilateral optic fibers into the vNAcSh of *VGAT-IRES-cre* mice (Fig. 2i). Animals were trained to receive pellets under a variable ITI schedule and their pellet consumption and head entries were recorded. Once animals consumed >50% of the pellets delivered and performed head entries more than the number of pellets delivered in a session, experimental and yellow fluorescent protein (YFP) control animals received stimulation for 12 s either side of reward delivery (Fig. 2j). On photoinhibition of VTA^{VGAT}-vNAcSh projections, we observed a trend toward a reduction in the total number of pellets consumed across counterbalanced sessions (Fig. 2k). In accordance with our prior results in which VTA^{VGAT}-vNAcSh was active during reward retrieval (head entries) (Fig. 1g,i-k and Extended Data Fig. 1c)

and sufficient for operant photoactivation (Fig. 2f), we found that photoinhibition with JAWS resulted in a significant reduction in the latency for pellet retrieval (Fig. 2l) and total reward-seeking-like events (that is, head entries), indicating that VTA^{VGAT}-vNAcSh projections are also necessary for promoting natural reward reinforcement (Extended Data Fig. 2p,q).

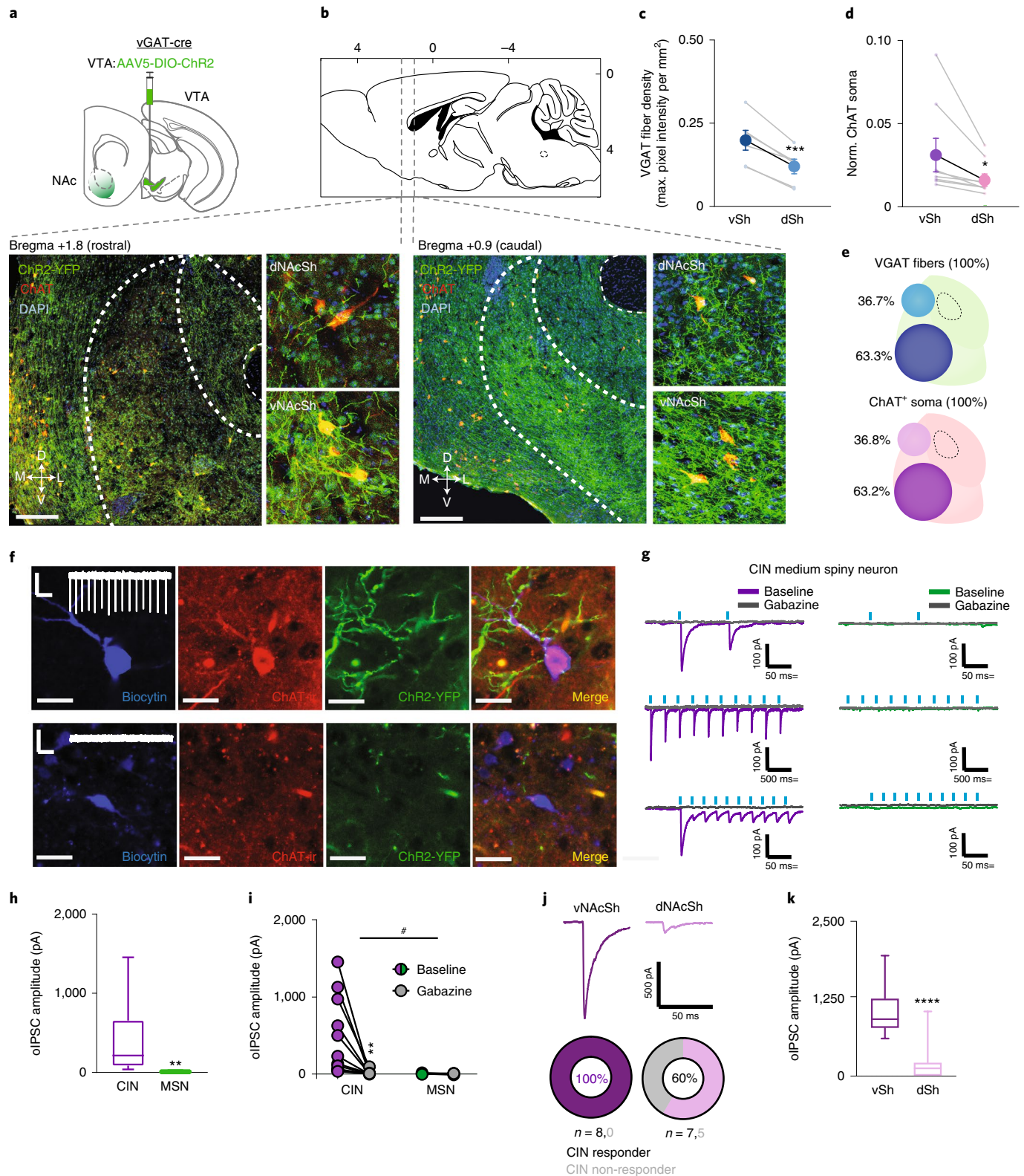
VTA GABAergic terminals preferentially project to, and inhibit, CINs in the vNAcSh. To better understand the differences in the magnitude of VTA^{VGAT}-NAc terminal activity in the vNAcSh and dNAcSh, and the selective reinforcing properties of VTA^{VGAT}-vNAcSh terminals, we implemented viral and transgenic tracing strategies to determine the density of VTA^{VGAT}-NAc projections across the NAc (Fig. 3a). In *VGAT-IRES-cre* mice injected with AAV5-DIO-ChR2-eYFP (where eYFP is enhanced YFP) into the VTA, we observed ChR2 expression across the mediolateral and rostrocaudal axis of the VTA (Extended Data Fig. 3a). In the NAc, we found a dorsal-to-ventral gradient in the density of NAcSh fibers across the rostrocaudal axis (Fig. 3b). We observed a significantly greater fluorescence intensity of VGAT fibers in the vNAcSh compared with the dNAcSh (Fig. 3c,e). In accordance with previous reports, we observed that VTA^{VGAT}-NAc fibers apposed the soma of CINs¹² (Fig. 3b) and we found a significantly larger number of ChAT⁺ soma in the vNAcSh compared with the dNAcSh (Fig. 3d,e).

We next determined the synaptic transmission of VTA^{VGAT}-NAc projections in the NAc. We tested whether these VTA^{VGAT}-vNAcSh projections form synapses on to the principal striatal neurons, the medium spiny neurons (MSNs), and/or on to CINs. We carried out *ex vivo*, whole-cell, patch-clamp recordings from putative CINs and MSNs, identified based on their morphological properties and the presence/absence of spontaneous activity in *VGAT-IRES-cre* transduced with AAV5-DIO-ChR2-eYFP in the VTA. In a subset of neurons, we filled them with biocytin and determined whether putative CINs were positive for choline acetyltransferase (ChAT) immunoreactivity (Fig. 3f). As expected, there was a marked difference in holding current between putative MSNs and CINs, reflecting known differences in resting membrane potential (Extended Data Fig. 3b). This established that we were accurately differentiating between CINs and MSNs. There was enhanced spontaneous inhibitory postsynaptic current (sIPSC) frequency (not amplitude) and tonic GABA current in CINs compared with MSNs, indicating

Fig. 3 | VTA GABAergic terminals preferentially project to, and inhibit, CINs in the vNAcSh. **a**, Coronal brain schematic of viral injection of ChR2 into the VTA and fiber expression in the NAc of *VGAT-Cre⁺* mice. **b**, Top: sagittal brain cartoon depicting the rostrocaudal position. Bottom: $\times 40$ confocal image of rostral NAc (left; +1.8 AP relative to Bregma) and caudal NAc (right; +0.9 AP relative to Bregma) showing expression of ChR2 (green), ChAT (red) and DAPI (blue). Scale, 100 μm . Zoomed images show expression of ChR2 fibers and ChAT soma in the dNAcSh (top) and vNAcSh (bottom). **c**, GABAergic fiber density (maximum pixel intensity mm^{-2}) in the vNAcSh or dNAcSh ($n=2$ mice, 6 slices; vNAcSh versus dNAcSh, paired Student's *t*-test, $P=0.0009$, $t=7.041$, d.f. = 5). Data are represented as mean \pm s.e.m., maximum. **d**, ChAT soma density (normalized (norm.) to DAPI) in the vNAcSh or dNAcSh ($n=2$ mice, 8 slices; vNAcSh versus dNAcSh, Student's paired *t*-test, $P=0.0264$, $t=2.329$, d.f. = 7). Data are represented as mean \pm s.e.m. **e**, Schematic depicting percentage of VGAT fiber density (top) and percentage of ChAT soma (relative to 100% total in the NAcSh; bottom) in the vNAcSh versus dNAcSh. **f**, Top: representative image of biocytin (blue), ChAT-ir (red) and ChR2-YFP (green) in the vNAcSh. Scale, 100 μm . White inset: spontaneous activity measured in cell-attached configuration. **g**, Example traces of evoked, whole-cell, voltage-clamp recordings of CIN activity (left) and MSN activity (right) in response to VTA-vNAcSh-vgat⁺ stimulation. **h**, Graph showing amplitude \pm s.e.m. of oIPSCs recorded in CINs and MSNs ($n=12$ CINs from 4 mice, 18 MSNs from 4 mice; CIN: minima = 38.8, maxima = 1,454, median = 214.6, range = 1,415, 25th percentile = 86.16, 75th percentile = 655.7, unpaired *t*-test, $t=3.132$, $^{**}P=0.0040$; MSN: minima = 2.02, maxima = 18.6, median = 7.489, range = 20.8, 25th percentile = 4.184, 75th percentile = 13.56). **i**, Graph showing change in amplitude \pm s.e.m. of oIPSCs recorded in CINs and MSNs with treatment of gabazine ($n=12$ CINs from 4 mice, 18 MSNs from 4 mice, two-way repeated-measure ANOVA: cell type \times time interaction: $F[1,18]=6.212$, $P=0.0227$; post-hoc Sidak's comparison of baseline versus gabazine: CIN: $P=0.0018$; MSN: $^{#}P=0.9996$). Data are represented as mean \pm s.e.m. **j**, Example traces of evoked, whole-cell, voltage-clamp recordings of CIN activity in response to ChR2 stimulation in the vNAcSh or dNAcSh, and plots of responders versus nonresponders in the vNAcSh (seven responders, no nonresponders) and dNAcSh (seven responders, five nonresponders). **k**, Graph showing amplitude \pm s.e.m. of oIPSCs recorded in CINs in the vNAcSh ($n=8$ cells, 4 mice, minima = -606.6, maxima = 1,946, median = 918.9, range = 1,339, 25th percentile = 774.8, 75th percentile = 1,257) versus dNAcSh ($n=12$ cells, 4 mice, minima = 0, maxima = 1,046, median = 126.4, range = 1,046, 25th percentile = 0, 75th percentile = 221.6) (unpaired *t* test, $^{****}P<0.0001$, $t=5.343$, d.f. = 18).

an overall enhanced GABAergic tone on CINs (Extended Data Fig. 3b). Photostimulation of VTA^{VGAT}-vNAcSh terminals in the NAcSh evoked robust IPSCs in CINs, but not MSNs (Fig. 3g,h), and this required activation of GABA_A-receptors because these IPSCs were fully blocked by gabazine (Fig. 3i), in accordance with other studies¹². Consistent with the frequency dependence of the stimulation for the behavioral response reported above, we found

that high-frequency stimulation of VTA^{VGAT}-vNAcSh terminals resulted in a summation of IPSCs (charge) on CINs (Extended Data Fig. 3c,d), indicative of enhanced GABAergic tone over time. To determine whether there were any potential differences in evoked IPSCs across dNAcSh to vNAcSh, we used ex vivo, whole-cell, patch-clamp recording in putative CINs from either the vNAcSh or the dNAcSh (Extended Data Fig. 3e,f). Further corroborating in vivo



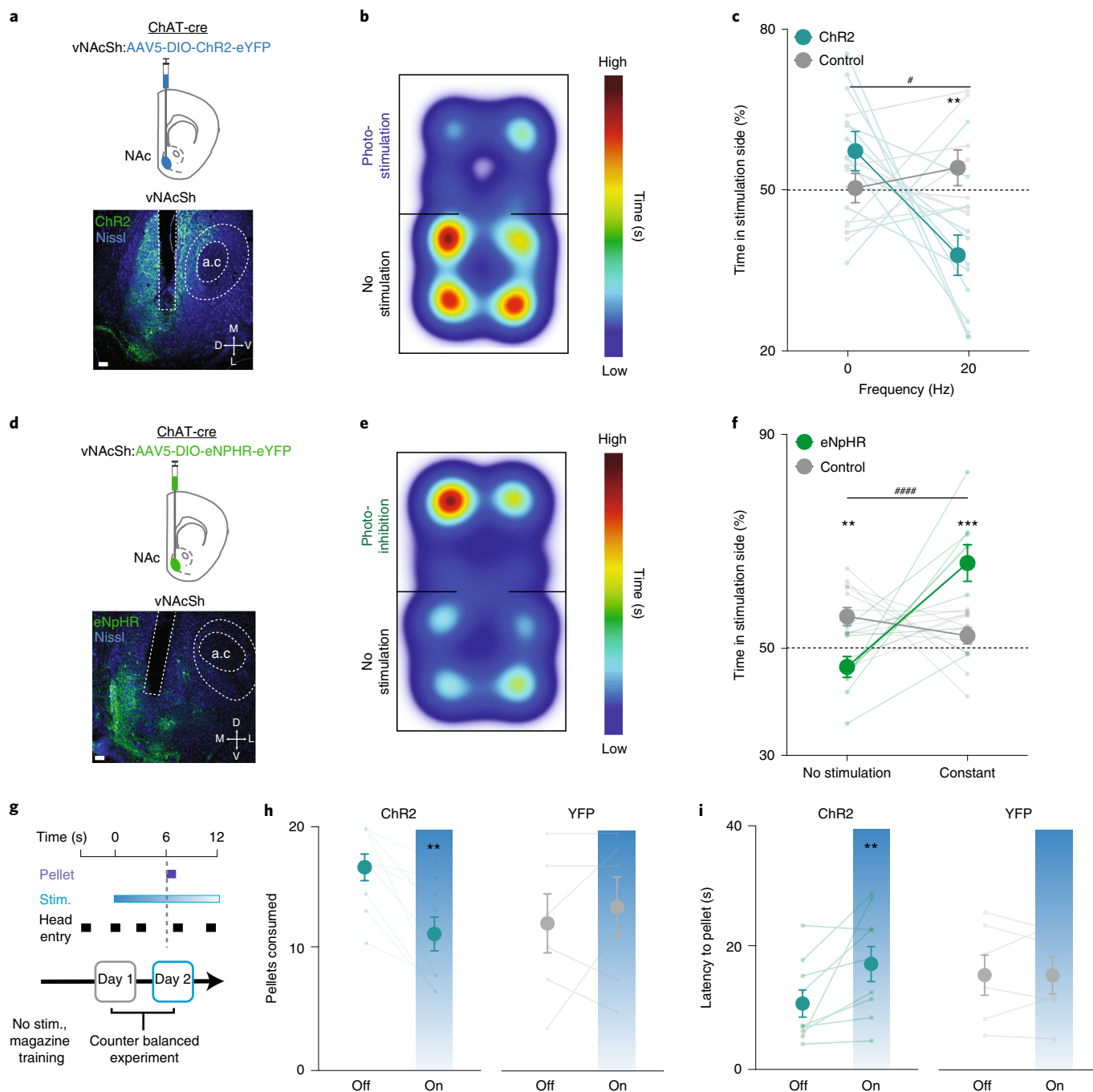


Fig. 4 | Photomanipulation of vNAcSh CIN activity bidirectionally modulates preference and reward reinforcement. **a**, Top: coronal brain schematic of viral injection of ChR2 into vNAcSh of *CHAT-Cre*⁺ mice. Bottom: representative $\times 20$ coronal image (left) showing expression of ChR2 (green), Nissl (blue) and fiber placement in vNAcSh (left). Scale, 100 μm . **b**, Representative heatmap raster plot showing behavioral response to ventral photoactivation. **c**, Significant aversion to vNAc photostimulation of ChAT neurons at 20 Hz. Two-way, repeated-measure ANOVA (control versus ChR2: $F[1,34]=4.729$, $P=0.0367$; 0 versus 20 Hz; $F[1,34]=1.718$, $P=0.1987$; interaction: $F[1,34]=10.41$, $*P=0.028$); Bonferroni's post-hoc test (ChR2 0 versus 20 Hz, $*P<0.0004$, $t=4.162$, $d.f.=34$; 20-Hz ChR2 versus control: $**P=0.0058$, $t=3.209$, $d.f.=34$). Data are represented as mean \pm s.e.m. ($n=8$ /control; 11/ChR2). **d**, Top: coronal brain cartoon of viral injection of eNpHR into vNAcSh of *CHAT-Cre*⁺ mice. Bottom: representative $\times 20$ coronal image (left) showing expression of eNpHR (green), Nissl (blue) and fiber placement in vNAcSh (left). Scale, 100 μm . **e**, Representative heatmap raster plot showing behavioral response to constant ventral photoinhibition. **f**, Real-time behavior after constant photoinhibition of ChAT neurons in ventral NAcSh (control versus eNpHR: $F[1,19]=5.182$, $P=0.0296$; 0 versus constant: $F[1,19]=10.66$, $P=0.0041$; interaction: $F[1,19]=22.65$, $####P=0.0001$); Bonferroni's post-hoc test (control versus eNpHR: $**P=0.0081$; control versus eNpHR: $***P=0.0002$). Data are represented as mean \pm s.e.m. ($n=8$ for control or 12 for eNpHR). **g**, Cartoon outlining experimental procedure of uncued reward delivery testing. **h**, Total pellets consumed in matched, counterbalanced sessions comparing laser on versus off (20 Hz, 5-ms pulse width). Left: ChR2 group ($n=9$ mice; off versus on, paired Student's t -test, $P=0.0014$, $t=4.797$, $d.f.=8$). Right: YFP group ($n=6$ mice; off versus on, paired Student's t -test, $P=0.4896$, $t=0.7454$, $d.f.=5$). Data are represented as mean \pm s.e.m. **i**, Pellet retrieval latencies in matched, counterbalanced sessions comparing laser on versus off (pulse 20 Hz). Left: ChR2 group ($n=9$ mice; off versus on, paired Student's t -test, $P=0.0275$, $t=2.690$, $d.f.=8$). Right: YFP group ($n=6$ mice; off versus on, paired Student's t -test, $P=0.9728$, $t=0.03587$, $d.f.=5$). Data are represented as mean \pm s.e.m.

photometry and optogenetic manipulation, we found that VTA^{VGAT} terminal photostimulation elicited significantly larger IPSC amplitudes in the vNAcSh, compared with the dNAcSh, and there was a greater preponderance for unresponsive (to VTA^{VGAT} photostimulation) CINs in the dNAcSh (Fig. 3j,k). Taken together, these results indicate that long-range VTA GABA projections selectively control CIN activity, and do so to a larger degree in the vNAcSh.

The vNAcSh CIN activity modulates reward processing.

We next identified the downstream mechanism by which the VTA^{VGAT}-vNAcSh projections enhance reward behaviors. It has been reported that VTA^{VGAT}-NAc synapses on CINs in this region facilitate aversive learning^{24–27}. Furthermore, prior optogenetic studies have reported that inhibition of NAc CINs does not drive a conditioned place preference²⁸ and inhibition of ChAT neurons in the medial NAc can suppress extinction learning in drug-associated contexts¹⁵. Studies have also reported that acetylcholine (ACh) signaling in the NAc decreases reward seeking and consumption; however, the role of vNAcSh CINs in natural reward behaviors is as yet unclear. We hypothesized that inhibition of CINs by vNAcSh projections may be necessary and sufficient for modulating natural reward-associated behaviors such as reward seeking and consumption. To directly test this hypothesis, we injected AAV5-DIO-ChR2-eYFP unilaterally or AAV5-DIO-eNpHR-eYFP bilaterally into the vNAcSh of *CHAT-IRES-cre* mice and implanted optic fibers into the vNAcSh (Fig. 4a,d). We found that photostimulation of vNAcSh^{ChAT} neurons induced a robust aversion behavior (Fig. 4b,c), whereas, conversely, photoinhibition of vNAcSh^{ChAT} neurons with constant illumination (and not phasic; Extended Data Fig. 4e,g) induced robust preference behaviors (Fig. 4e,f). The latter result supports our results from direct stimulation of VTA^{VGAT}-vNAcSh projections (Fig. 2b), suggesting that either activation of VTA^{VGAT}-vNAcSh projections or inhibition of vNAcSh^{ChAT}

neurons can result in the promotion of real-time place preference behavior. In addition, we assessed the role of vNAcSh^{ChAT} photoactivation in self-stimulation and found no increase in nose pokes for light stimulation relative to controls (Extended Data Fig. 4c), suggesting that the activation of vNAcSh^{ChAT} neurons is not by itself reinforcing.

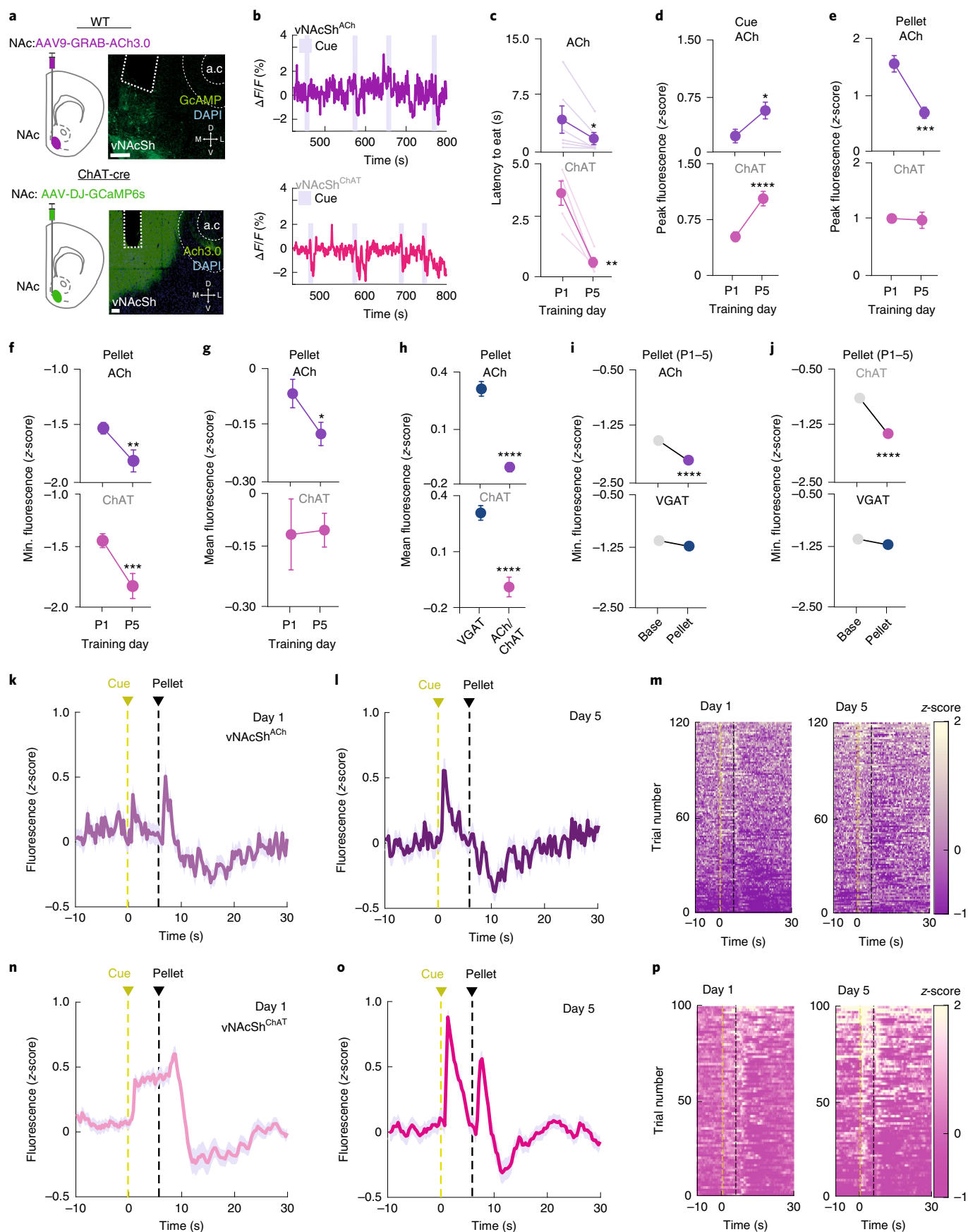
These results highlight the functional importance of the VTA^{VGAT}-vNAcSh^{ChAT} circuit, wherein VTA^{VGAT}-vNAcSh activity is engaged to inhibit vNAcSh^{ChAT} activity and subsequent ACh release during natural reward-associated behaviors. We previously found (Fig. 2k,l) that inhibition of VTA^{VGAT}-vNAcSh terminals resulted in a marked reduction in positively reinforcing, head-entry behaviors. Thus, we next hypothesized that VTA^{VGAT}-vNAcSh acting on vNAcSh^{ChAT} neurons would promote behaviors downstream of reward seeking, that is, reward consumption. Thus, we tested the effects of photoactivation of vNAcSh^{ChAT} cell bodies in a noncued reward delivery task (Fig. 4g). Similar to inhibited VTA^{VGAT}-vNAcSh activity (Fig. 2k,l), photoactivation of vNAcSh^{ChAT} cell bodies resulted in a significant decrease in the pellets consumed (Fig. 4h), an increase in the latency to retrieve the consumed pellets (Fig. 4h) and a trend toward a decrease in reward-seeking-like ITI head entries (Extended Data Fig. 4h). This result indicates that vNAcSh^{ChAT} inhibition is necessary for promoting reinforcement to natural reward, specifically reward consumption.

CIN activity and ACh release in the vNAcSh are inhibited during reward reinforcement. To address whether and how vNAcSh^{ChAT} neuron activity and subsequent ACh release are engaged during reward reinforcement, we recorded ACh release and CIN neuronal activity in the vNAcSh or the dNAcSh using fiber photometry during pavlovian and operant conditioning (Fig. 1b,c and Extended Data Fig. 1i). We used either the modified ACh biosensor²⁹ (GRAB-ACh3.0) by injecting AAV9-GRAB-ACh3.0 in

Fig. 5 | CIN activity and ACh release in the vNAcSh are inhibited during reward reinforcement. **a**, Left: coronal brain cartoon (top) of viral injection of either GRAB-ACh3.0 (top) or GcAMP6s (bottom) into the vNAcSh of WT mice. Right: representative coronal image showing expression of GcAMP6s (green), DAPI (blue) and fiber placement (top), or GRAB-ACh3.0 (green), DAPI (blue) and fiber placement (bottom) in the vNAcSh. Scale, 200 μ m. **b**, Representative recorded activity in the vNAcSh for GRAB-ACh3.0 (top) or GcAMP6s (bottom) (highlights represent cue light during reward period). **c**, Latency to eat after reward delivery (0–6 s) for pavlovian training. Top: vNAcSh GRAB-ACh3.0 ($n = 6$ mice; P1 versus P5, paired Student's *t*-test, $^*P = 0.0302$, $t = 2.416$, d.f. = 5). Bottom: vNAcSh ChAT GcAMP6s ($n = 5$ mice; P1 versus P5, paired Student's *t*-test, $^{**}P = 0.0038$, $t = 6.201$, d.f. = 4). Data are represented as mean \pm s.e.m. **d**, Peak fluorescence during cue period (0–6 s) for pavlovian training. Top: vNAcSh GRAB-ACh3.0 ($n = 6$ mice; P1 versus P5, paired Student's *t*-test, $^*P = 0.0122$, $t = 2.546$, d.f. = 114). Bottom: vNAcSh ChAT GcAMP6s ($n = 5$ mice; P1 versus P5, paired Student's *t*-test, $^{***}P < 0.0001$, $t = 4.355$, d.f. = 95). Data are represented as mean \pm s.e.m. **e**, Peak fluorescence during reward period (6–30 s) for pavlovian training. Top: vNAcSh GRAB-ACh3.0 ($n = 6$ mice; P1 versus P5, paired Student's *t*-test, $^{***}P < 0.0001$, $t = 5.424$, d.f. = 114). Bottom: vNAcSh ChAT GcAMP6s ($n = 5$ mice; P1 versus P5, paired Student's *t*-test, $P = 0.4182$, $t = 0.8140$, d.f. = 95). Data are represented as mean \pm s.e.m. **f**, Minimum fluorescence during reward period (6–30 s) for pavlovian training. Top: vNAcSh GRAB-ACh3.0 ($n = 6$ mice; P1 versus P5, paired Student's *t*-test, $^{**}P = 0.0077$, $t = 2.711$, d.f. = 114). Bottom: vNAcSh ChAT GcAMP6s ($n = 5$ mice; P1 versus P5, paired Student's *t*-test, $^{***}P = 0.0001$, $t = 4.038$, d.f. = 95). Data are represented as mean \pm s.e.m. **g**, Mean fluorescence during reward period (6–30 s) for pavlovian training. Top: vNAcSh GRAB-ACh3.0 ($n = 6$ mice; P1 versus P5, paired Student's *t*-test, $^*P = 0.0355$, $t = 2.128$, d.f. = 114). Bottom: vNAcSh ChAT GcAMP6s ($n = 5$ mice; P1 versus P5, paired Student's *t*-test, $P = 0.8999$, $t = 0.1263$, d.f. = 95). Data are represented as mean \pm s.e.m. **h**, Mean fluorescence comparison during reward period (6–30 s) for pavlovian training. Top: vNAcSh GRAB-ACh3.0 versus vNAcSh VGAT terminal GcAMP6s (unpaired Student's *t*-test, $^{****}P < 0.0001$, $t = 8.513$, d.f. = 529). Bottom: vNAcSh ChAT GcAMP6s versus vNAcSh VGAT terminal GcAMP6s (unpaired Student's *t*-test, $^{****}P < 0.0001$, $t = 6.007$, d.f. = 451). Data are represented as mean \pm s.e.m. **i**, Minimum fluorescence comparison for baseline (–10 to 0 s) and reward period (6–30 s) during all pavlovian training days. Top: GRAB-ACh3.0 ($n = 6$ mice; paired Student's *t*-test, $^{****}P < 0.0001$, $t = 9.185$, d.f. = 385). Bottom: vNAcSh VGAT terminal GcAMP6s ($n = 7$ mice; paired Student's *t*-test, $P < 0.1886$, $t = 1.318$, d.f. = 298). Data are represented as mean \pm s.e.m. **j**, Minimum fluorescence comparison for baseline (–10 to 0 s) and reward period (6–30 s) during all pavlovian training days. Top: vNAcSh ChAT GcAMP6s ($n = 6$ mice; paired Student's *t*-test, $^{****}P < 0.0001$, $t = 7.85$, d.f. = 230). Bottom: vNAcSh VGAT terminal GcAMP6s ($n = 7$ mice; paired Student's *t*-test, $P < 0.1886$, $t = 1.318$, d.f. = 298). Data are represented as mean \pm s.e.m. **k**, Mean vNAcSh GRAB-ACh3.0-recorded calcium activity averaged across all trials from day 1 of pavlovian conditioning ($n = 6$ mice). Data are represented as mean \pm s.e.m. **l**, Mean vNAcSh GRAB-ACh3.0-recorded calcium activity averaged across all trials from day 5 of pavlovian conditioning ($n = 6$ mice). Data are represented as mean \pm s.e.m. **m**, Heatmap raster plot of vNAcSh GRAB-ACh3.0-recorded calcium activity for every trial of pavlovian conditioning on day 1 (left) and day 5 (right). Trials are displayed in ascending order by average activity after pellet delivery ($n = 6$ mice). **n**, Mean vNAcSh ChAT GcAMP6s-recorded calcium activity averaged across all trials from day 1 of pavlovian conditioning ($n = 5$ mice). Data are represented as mean \pm s.e.m. **o**, Mean vNAcSh ChAT GcAMP6s-recorded calcium activity averaged across all trials from day 5 of pavlovian conditioning ($n = 5$ mice). Data are represented as mean \pm s.e.m. **p**, Heatmap raster plot of vNAcSh ChAT GcAMP6s-recorded calcium activity for every trial of pavlovian conditioning on day 1 (left) and day 5 (right). Trials are displayed in ascending order by average activity after pellet delivery ($n = 5$ mice).

WT mice, or GcAMP6s by injecting AAVDJ-DIO-GCaMP6s in *CHAT-IRES-cre* mice, into the vNAcSh (Fig. 5a). We next implanted an optical fiber in the vNAcSh and recorded either GRAB-ACh3.0

activity or GCaMP activity of vNAcSh^{CHAT} neurons while animals underwent pavlovian and then operant conditioning. All animals showed a decreased latency to begin pellet consumption across



pavlovian conditioning (Fig. 5b), and a reduction in unrewarded, ITI head entries throughout training (Extended Data Fig. 5b,f). Furthermore, we found an increase in GRAB-ACh3.0 and ChAT GCaMP activity primarily to cue and pellet delivery (Fig. 5c). During cue presentation, we found increased GRAB-ACh3.0 activity and ChAT GCaMP activity on all training days, with an increase in peak fluorescence across conditioning (Fig. 5d,k–p). Immediately on pellet delivery, we observed an increase in peak fluorescence in both GRAB-ACh3.0 (Fig. 5k–m) and ChAT GCaMP (Fig. 5n–p). It is interesting that this peak activity decreased as animals progressed through pavlovian conditioning, with a significant reduction in GRAB-ACh3.0 peak fluorescence on day 5 compared with day 1 (Fig. 5e). Furthermore, we found a marked and significant inhibition in GRAB-ACh3.0 (Fig. 5k–m and Extended Data Fig. 5c) and ChAT GCaMP activity (Fig. 5n–p and Extended Data Fig. 5g) immediately after pellet retrieval during pellet consumption, and no appreciable changes in fluorescence during ITI head entries (Extended Data Fig. 5d,h). This inhibition, when measured as the minimum fluorescence response (GRAB-ACh3.0 or ChAT GCaMP) to pellet consumption, is strongest on day 5 relative to day 1 (Fig. 5f). The reduction in the peak fluorescence on pellet delivery (Fig. 5e), and the inhibition during consumption (Fig. 5f), resulted in an overall reduction in the mean fluorescence during the reward reinforcement period. This reduction encompassed the periods of pellet delivery, retrieval and consumption (Fig. 5g). In contrast to GCaMP activity in VTA^{VGAT}-vNacSh terminals, we observed a decrease in mean fluorescence activity during reward reinforcement (Fig. 5h). Moreover, unlike GRAB-ACh3.0 activity, or GCaMP activity in ChAT soma, we found no significant changes in minimum fluorescence from baseline at VTA^{VGAT}-vNacSh projections during the reward reinforcement period (Fig. 5i,j). Together, these results collectively support the conclusion that vNacSh^{CHAT} neuron activity and subsequent ACh release are inhibited during reward reinforcement, in apparent contrast to the increase in VTA^{VGAT}-vNacSh activity during the same behavioral epoch. Moreover, during pavlovian extinction, reward omission eliminated the increase to

pellet delivery and decrease in activity to reward consumption in both GRAB-ACh3.0 and ChAT GCaMP recordings (Extended Data Fig. 5k,l).

Similar patterns of activity were observed during operant conditioning in vNacSh when measuring both ACh release (GRAB-ACh3.0) and GCaMP activity in vNacSh^{CHAT} neurons. Both groups of animals had more nosepoke behavior on day 3 of FR-1 compared with day 1 (Extended Data Fig. 5m), and enhanced peak fluorescence activity to cues (Extended Data Fig. 5n,q–t), sustained maximal activity after pellet delivery (Extended Data Fig. 5o,q–t) and a marked inhibition in activity, as measured by the minimum fluorescence during reward consumption (Extended Data Fig. 5p,q–t).

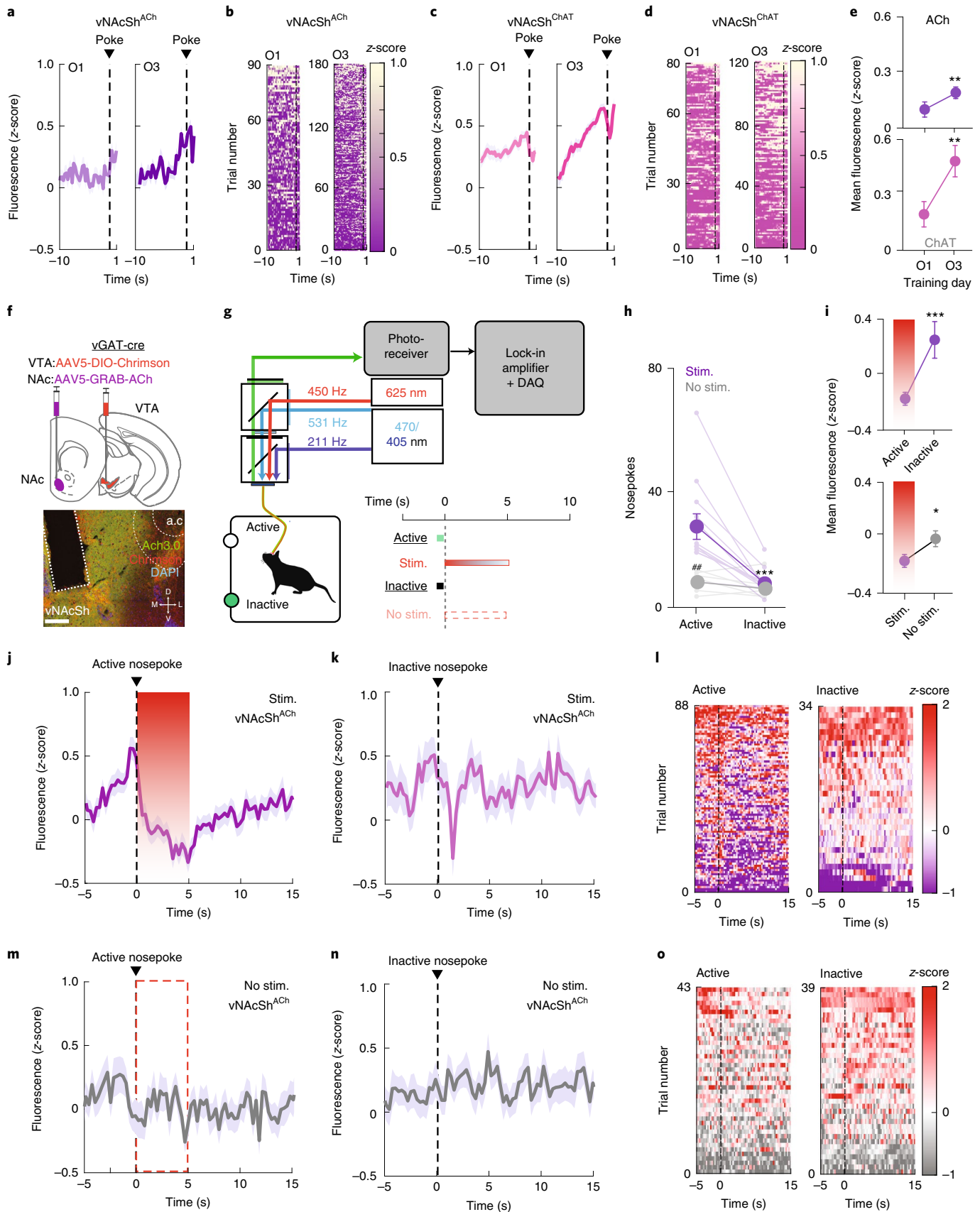
GRAB-ACh3.0 recordings were also used in the dNacSh while animals underwent pavlovian and operant conditioning. In this experiment, dNacSh^{ACh} mice showed reduced latency to pellet retrieval and increased active nosepokes across pavlovian and operant conditioning, respectively (Extended Data Fig. 6b). Unlike vNacSh, peak GRAB-ACh3.0 activity showed no change during cue presentation (Extended Data Fig. 6c), no reduction on pellet delivery (Extended Data Fig. 6d) and, opposite to what we observed in the vNacSh, an increase in minimum fluorescence (Extended Data Fig. 6e) across pavlovian or operant conditioning phases. Similar to the findings in VTA^{VGAT}-NacSh terminal GCaMP recordings (Fig. 1h and Extended Data Fig. 1f), we observed a significantly smaller magnitude in GRAB-ACh3.0 activity (Extended Data Fig. 6g–j), notably when comparing the minimum fluorescence during reward consumption activity in dNacSh^{ACh} with that in vNacSh^{ACh} (Extended Data Fig. 6f). These results, in combination with our optogenetic manipulations (Fig. 4h,i), support the conclusion that vNacSh^{CHAT} neurons are inhibited by VTA^{VGAT}-vNacSh activity during natural reward reinforcement.

Acetylcholine release in vNacSh is inhibited by VTA^{VGAT}-vNacSh activity. Thus far, our results indicate opposing patterns of activity during natural reward reinforcement behaviors in VTA^{VGAT}-vNacSh terminals, compared with the dynamic ChAT neuron activity and

Fig. 6 | ACh release in the vNacSh is inhibited by VTA-vNacSh^{VGAT} activity. **a**, Mean vNacSh GRAB-ACh3.0-recorded calcium activity preceding a nosepoke averaged across all trials from day 1 (left) and day 3 (right) of operant conditioning ($n = 6$ mice). Data are represented as mean \pm s.e.m. **b**, Heatmap raster plot of vNacSh GRAB-ACh3.0-recorded calcium activity preceding a nosepoke for every trial of operant conditioning on day 1 (left) and day 3 (right). Trials are displayed in ascending order by average activity preceding a nosepoke ($n = 6$ mice). **c**, Mean vNacSh ChAT GCaMP6s-recorded calcium activity preceding a nosepoke averaged across all trials from day 1 (left) or day 3 (right) of operant conditioning ($n = 6$ mice). Data are represented as mean \pm s.e.m. **d**, Heatmap raster plot of vNacSh ChAT GCaMP6s-recorded calcium activity preceding a nosepoke for every trial of operant conditioning on day 1 (left) and day 3 (right). Trials are displayed in ascending order by average activity preceding a nosepoke ($n = 5$ mice). **e**, Mean fluorescence during nosepoke ramp (–10 to 1 s) for operant (O) training days. Top: vNacSh GRAB-ACh3.0 pavlovian days ($n = 6$ mice; O1 versus O3, paired Student's t -test, $**P = 0.0012$, $t = 3.35$, d.f. = 85). Bottom: vNacSh ChAT GCaMP6s operant days ($n = 5$ mice; O1 versus O3, paired Student's t -test, $**P = 0.0048$, $t = 2.879$, d.f. = 109). Data are represented as mean \pm s.e.m. **f**, Coronal brain cartoon (top) of viral injection of Chrimson into the VTA and GRAB-ACh4.3 into the vNacSh of VGAT-Cre⁺ mice, and representative $\times 40$ coronal image (bottom panel) showing expression of GRAB-ACh4.3 (green), Chrimson (red) and DAPI (blue) in the vNacSh. **g**, Cartoon schematic of fiber photometry setup connected to mouse performing operant task where active nosepoke results in 40-Hz red light stimulation. **h**, Total nosepokes performed (active versus inactive) in counterbalanced sessions resulting in Chrimson stimulation and no stimulation ($n = 6$ mice, two-way ANOVA, $***$ active versus inactive in stimulation (stim.): $P = 0.0001$, $t = 4.982$, d.f. = 32; $##$ active stimulation versus active no stimulation: $P = 0.0022$, $t = 3.979$, d.f. = 32). Data are represented as mean \pm s.e.m. **i**, Top: mean vNacSh GRAB-ACh3.0 fluorescence comparison across active (resulting in Chrimson stimulation) versus inactive nosepoke trials ($n = 6$ mice, unpaired Student's t -test, $***P = 0.0002$, $t = 3.844$, d.f. = 119). Bottom: mean vNacSh GRAB-ACh3.0 fluorescence comparison of active nosepoke trials across stimulation (resulting in Chrimson stimulation) versus no stimulation days ($n = 6$ mice, unpaired Student's t -test, $*P = 0.0436$, $t = 2.309$, d.f. = 126). Data are represented as mean \pm s.e.m. **j**, Mean vNacSh-recorded GRAB-ACh3.0 activity during the stimulation session averaged across all active (resulting in Chrimson stimulation) nosepoke trials ($n = 6$ mice). Data are represented as mean \pm s.e.m. **k**, Mean vNacSh-recorded GRAB-ACh3.0 activity during the stimulation session averaged across all inactive (resulting in Chrimson stimulation) nosepoke trials ($n = 6$ mice). Data are represented as mean \pm s.e.m. **l**, Heatmap raster plot of vNacSh-recorded GRAB-ACh3.0 activity for every active nosepoke trial (resulting in Chrimson stimulation). Trials are displayed in ascending order by mean activity during active nosepokes ($n = 6$ mice). **m**, Mean vNacSh-recorded GRAB-ACh3.0 activity during the no stimulation session averaged across all active (resulting in no Chrimson stimulation) nosepoke trials ($n = 6$ mice). Data are represented as mean \pm s.e.m. **n**, Mean vNacSh-recorded GRAB-ACh3.0 activity during the no stimulation session averaged across all inactive (resulting in no Chrimson stimulation) nosepoke trials ($n = 6$ mice). Data are represented as mean \pm s.e.m. **o**, Heatmap raster plot of vNacSh-recorded GRAB-ACh3.0 activity for every active nosepoke trial (resulting in no Chrimson stimulation). Trials are displayed in ascending order by mean activity during active nosepokes ($n = 6$ mice).

subsequent ACh release. It is of interest that, during our recordings of GRAB-ACh3.0 or ChAT GCaMP activity across operant conditioning, we found a significant increase in CIN activity and

ACh release immediately preceding a nosepoke during instrumental training (Fig. 6a–e), whereas VTA^{VGAT}-vNacSh terminals showed no increased GCaMP activity (Extended Data Fig. 1g,h).



On reinforcement of the nosepoke with a natural reward, we observed a marked reduction in GRAB-ACh activity (Fig. 5g) and, in contrast, an increase in GCaMP activity from the VTA^{VGAT}-vNacSh projections (Fig. 1g). Based on these results, we hypothesized, together with our ex vivo electrophysiology results (Fig. 3j,k), that VTA^{VGAT}-vNacSh terminals cause a direct inhibition of ACh release to promote reinforcement behavior. To directly test this, we determined the sufficiency for VTA^{VGAT}-vNacSh terminals to inhibit ACh release dynamics in vivo. We injected the red shifted opsin ChrimsonR³⁰, using AAV5-DIO-ChrimsonR-tdTomato in the VTA and AAV9-GRAB-ACh3.0 in the vNacSh of vGAT-IRES-cre mice, and implanted a photometry fiber in the vNacSh (Fig. 6f). We implemented a modified operant task on an FR-1 schedule, where an active nosepoke resulted in the photoactivation of VTA^{VGAT}-vNacSh terminals via ChrimsonR photoactivation in counterbalanced sessions (Fig. 6g). Importantly, animals performed significantly higher active nosepokes within a stimulation session, and significantly more active nosepokes in a stimulation session compared with a nonstimulation session (where an active nosepoke resulted in no stimulation; Fig. 6h,i). Similar to what we observed in instrumental responding for a natural reward (Fig. 6a–e), we observed an increase in GRAB-ACh3.0 activity preceding active nosepoke for ChrimsonR-mediated VTA^{VGAT}-vNacSh terminals, followed by a marked, prolonged inhibition on photoactivation of ChrimsonR in vivo (Fig. 6j,l). Conversely, we saw no significant, prolonged inhibition in GRAB-ACh3.0 dynamics when animals made inactive nosepokes within the same session, or when the active nosepoke yielded no red-laser stimulation in counterbalanced sessions (Fig. 6k,m–o). Altogether, these results demonstrate an inverse relationship between VTA^{VGAT}-vNacSh terminal activity and vNacSh^{CHAT} neuron or ACh release dynamics, implicating VTA^{VGAT}-vNacSh projections directly in the inhibition of vNacSh^{CHAT} neurons during natural reward reinforcement behavior.

Discussion

Mesolimbic circuits have long been implicated in reward-related and motivated behaviors. Much of the attention has focused on mesolimbic DA projections, specifically from the VTA to the NAc³¹. More recently, a population of long-range GABAergic projections from the VTA to multiple limbic structures, including the NAc, had been described^{8,12,32}. Within the NAc, studies have established that VTA^{VGAT}-NAc neurons project specifically to CINs and are involved in aversive learning^{12,33}. However, these studies do not distinguish across the rostrocaudal^{19,20}, mediolateral²¹ and dorsoventral¹⁷ axes of the NAcSh, in which behavioral and functional heterogeneity has been shown by several groups, including ours. In the present study, we sought to determine whether VTA^{VGAT}-NAc neurons across dorsal and ventral NAc subregions differentially regulate reward-related behaviors.

A dorsoventral gradient for VTA-NAc GABAergic projections.

We reported that VTA^{VGAT}-NAc neuronal activity is engaged during reward-associated behaviors, with a distinct structural and functional gradient across the dorsoventral axis of the NAc. Specifically, VTA^{VGAT}-vNacSh neuronal activity correlated with cue and reward behaviors in both the ventral and the dorsal NAcSh. Our findings extended beyond these to show that VTA^{VGAT}-NAc neuronal activity to a cue or in anticipation of a reward increased during conditioning in the dNacSh. However, increases in VTA^{VGAT}-NAc neuronal activity during reinforcement to reward (reward delivery, retrieval and consumption) were restricted to the vNacSh. We found that VTA^{VGAT}-vNacSh projections were engaged during cue presentations, reward delivery, retrieval and consumption, albeit to varying degrees. Importantly, we showed an increased density in VGAT fibers, in the vNacSh, compared with the dNacSh. We also

reported that photostimulation of VTA^{VGAT}-vNacSh terminals (and not dNacSh or NAcC) is sufficient to promote preference behavior and self-stimulation, whereas photoinhibition studies result in a reduction in general reward-seeking-like behavior and latency to retrieve pellets, thereby corroborating our photometry results. Together, our findings identified distinct functional roles for VTA^{VGAT}-vNacSh projection in reward cue/anticipation versus reward retrieval/consumption in the dNacSh and vNacSh, respectively. It is interesting that these findings parallel the physiological signature of DA in the NAc more broadly where studies have shown engagement of VTA-NAc dopaminergic projection after a reward and anticipatory cues preceding the reward¹. In contrast, there is evidence to show that direct activation of VTA GABAergic projections to the NAc did not alter reward consumption³², although this study focused on the core and not the NAcSh or regions therein. A recent study also showed that stress-induced reductions in reward consumption are mediated by VTA GABA neurons, although this was not conducted in a projection-specific or subregion-targeted manner³⁴. This is further complicated by an important recent report investigating the effects of glutamate inputs to various regions in the NAc, which found opposing patterns in activity in the rostral versus the caudal NAcSh during reward consumption¹⁹. These cell-type, regional and functional differences in NAc reward processing highlight that we still do not fully understand how VTA^{VGAT}-NAc projections might control DA dynamics in the NAc and subsequent DA-related behaviors, and future studies are warranted.

VTA GABA projections promote positive reinforcement via inhibition of CINs. To further explore how long-range VTA GABAergic projections drive positive reinforcement, we investigated CINs, to which, it has previously been shown, VTA GABA projections exclusively synapse¹². In the present study, we both corroborate and extend these findings in several important areas. We found that VTA^{VGAT}-vNacSh projections inhibit vNacSh CINs to a greater degree than dNacSh, as evidenced by a greater density of fibers and number of ChAT⁺ soma in the vNacSh. These results translate in vivo, where, similar to VTA^{VGAT}-vNacSh activation, we show that vNacSh^{CHAT} inhibition drives place-preference behaviors. This is in contrast to photoactivation of vNacSh^{CHAT} neurons that drive a place aversion and a reduction in reward consumption. It is important to highlight here that VTA^{VGAT}-vNacSh inhibition disrupts general reward seeking and reward retrieval, whereas perturbing the downstream control of this circuit on vNacSh^{CHAT} neurons affects a behavior downstream of reward seeking/retrieval, that is, reward consumption.

CIN activity and ACh signaling in the striatum have been shown to play critical roles in motivation and reward. Prior studies have identified pauses in CIN firing during salient cues³⁵ and reward reinforcement³⁶, a function primarily ascribed to the bidirectional control ACh and DA exert over each other³⁷. ACh can potentiate (or depress, in some cases) DA release via actions at both muscarinic and nicotinic ACh receptors on DA axons³⁸. Conversely, DA release can coordinate the activity of CINs via its actions on D₂ receptors³⁹, resulting in the potentiation of drug preference⁴⁰. Once again, complex, and as yet unclarified, distinctions arise when considering the compartments of the striatum. For example, ACh regulation of DA release is distinct in the NAcSh compared with the NAcC and the dorsal striatum⁴¹ and, conversely, DA signaling elicits a burst in CIN firing in the NAcSh, while doing the opposite (pause) in the rest of the striatum⁴². Hence, in the present study, we ascertained CIN activity and ACh release across the NAc gradient during natural reward reinforcement behaviors.

In assessing how natural ACh release dynamics in vivo are involved in reward reinforcement and regulated by VTA^{VGAT}-vNacSh activity, we utilized a new ACh sensor to assay neuromodulator

dynamics (GRAB-ACh3.0)²⁹. Importantly, using this tool we found that GRAB-ACh dynamics were highly correlated with ChAT GCaMP activity during the same behavioral epochs. We also observed that vNacSh^{ChAT}/vNacSh^{ACh} activity is inversely correlated with VTA^{VGAT}-vNacSh activity during natural reward reinforcement. Specifically, we found that there was an increase in vNacSh^{ChAT}/vNacSh^{ACh} activity, but not dNacSh, to reward anticipatory cues, and a strengthening of peak sensor fluorescence across pavlovian conditioning. Previous studies have demonstrated an important role for ACh signaling in the striatum in motivation and reward seeking; however most of these studies suggest that CINs pause their activity in response to salient cues^{35,36,43}. However, it is important to consider that: (1) most of these studies have been conducted in the NAcC or the dorsal striatum; indeed recent *ex vivo* studies highlight important distinctions in how CINs regulate DA release in the NAcSh versus the rest of the striatum⁴¹; and (2) these studies assessed CIN activity using single-unit recordings, thereby limiting their ability to understand CIN activity and concurrent ACh release dynamics at the population level.

Some studies have reported that NAc ACh signaling decreases natural and drug reward seeking^{44,45} and reward consumption⁴⁶. In addition, increased NAc-CIN activity causes a reduction in palatable food consumption⁴⁵. Consistent with these studies, we showed a reduction in vNacSh^{ChAT}/vNacSh^{ACh} activity on pellet delivery across pavlovian conditioning, which directly opposed what we observed in the VTA^{VGAT}-vNacSh terminals. There was also marked inhibition during pellet retrieval and consumption inversely correlated to the increases observed in VTA^{VGAT}-vNacSh terminals, converse to the increased activity we observe in the VTA^{VGAT}-vNacSh projection. These results are further corroborated by the photoactivation experiments whereby vNacSh^{ChAT} photoactivation disrupted reward consumption, and are in accordance with increased CIN activity during the completion of motivated behaviors⁴⁷. The dNacSh^{ACh} dynamics on pellet delivery were unchanged and there was smaller inhibition in fluorescence to pellet consumption, compared with vNacSh^{ACh}, suggesting that this VTA^{VGAT}-vNacSh^{ChAT} interaction is selective for this important NAc subregion, and further highlights the heterogeneous nature of the NAc across the dorsoventral and anteroposterior axis, in line with our and other recent reports^{17–21}.

Perhaps an equally important finding from this report is that ChAT neurons and subsequent ACh release are engaged during an instrumental response, in our case nose-poking. This is apparent as a ‘ramp’ in activity preceding the nose-poke, with the fluorescence intensity (for ChAT GCaMP and GRAB-ACh3.0) peaking at the action. It is notable that VTA^{VGAT}-vNacSh terminal activity is largely quiescent during operant action, a departure from classic DA terminal responses to the instrumental responses shown in the NAc^{2,48}. Given the role of CINs in facilitating the release⁴⁹ and controlling reward-related behaviors²⁸, the existence of ‘ramp’-like patterns of activity in striatal MSNs to reward approach and seeking⁵⁰, it is possible that CIN modulation promotes an action-related component of reward seeking. This process would then be independent of their upstream interactions with VTA^{VGAT}-vNacSh inputs, either by exerting effects directly on DA terminals⁵¹ or via their regulation of MSN activity²⁸. After this, it is tempting to speculate that vNacSh CIN inhibition may ‘prime’ the downstream MSNs to more efficiently respond to dopaminergic responses and effect reward-related behaviors. Future, careful studies are required, using multi-color photometry or combinatorial photometry–electrophysiological studies, to determine how ACh signaling, DA release dynamics and MSN activity work together in concert to coordinate reward reinforcement behaviors.

Important to the present study, we also found *in vivo* that VTA^{VGAT}-vNacSh stimulation is sufficient to cause a long-lasting,

significant inhibition of ACh release *in vivo* at timescales similar to that induced during reward consumption bouts. We observed, in counterbalanced sessions, that animals engage in more instrumental responses that yielded them stimulation, consistent with our results that VTA^{VGAT}-vNacSh photoactivation is reinforcing. This finding corroborates the present study and the themes highlighted in this discussion, future studies will focus on how the VTA^{VGAT}-NacSh^{ChAT} circuit specifically mediates DA terminal release to control the various components of reward reinforcement behavior.

It is important to recognize that, although signals for GRAB-ACh3.0 and ChAT GCaMP are largely correlated across reward delivery, retrieval and consumption, there are some distinctions wherein there is a sustained increase across pavlovian conditioning during pellet delivery in the ChAT GCaMP group that is not observed with GRAB-ACh3.0 in the vNacSh. Changes in GCaMP6s activity reflect fluctuations in intracellular Ca²⁺ levels, which may be quite different to actual neurotransmitter release (or in this case a reduction in release). Furthermore, the kinetics of GCaMP6s may be different to GRAB sensors, and it is imperative to take all these distinctions into careful consideration when comparing changes in GCaMP6s and GRAB sensors as proxies for neuronal activity and neurotransmitter release, respectively. It is also important to note that the vNacSh is immediately adjacent to the diagonal band (DBB), part of the larger basal forebrain, a CIN-rich region (perhaps more than the NAcSh)⁵². Furthermore, CINs are probably the primary source of ACh in the NAcSh, but may not be the only source⁵³. Given the shortcomings with regard to the specificity of fiber photometry, it is possible that we are also sampling some ChAT neuron activity and ACh release from part of the DBB (and the brainstem as an external source of ACh), a limitation that will be resolved using higher-resolution, single-cell imaging techniques. Previous studies involving the DBB have implicated a role for these neurons (and the region) in attention⁵⁴ and cognition⁵⁵; however, it will be important for future studies to assay the DBB's role in reward and motivation and delineate its contribution from the NAcSh.

Multiple studies have shown that mesolimbic circuitry, and the NAc in particular, are hijacked by mental illness, notably, substance use disorders⁵⁶ and depression⁶, among others. However, much of the emphasis has been on how drugs of abuse or behaviorally modeled facets of mental illness affect NAc MSNs⁵⁷ or the glutamatergic inputs into the NAc⁵⁸. Furthermore, although studies have focused on NAcC versus NAcSh distinctions with respect to drugs of abuse⁵⁹, a systematic delineation of whether distinct subregions of the NAc are differentially impacted in disease is lacking. Congruently, aberrant striatal CIN activity and ACh signaling have also been implicated in drug reinforcement^{40,60,61} and depression^{62,63}, yet, how perturbations in ACh dynamics across the NAc contribute to neuropsychiatric diseased states is unclear. Hence, future studies are required to uncover the effects of diseased states on VTA^{VGAT}-Nac projections and their regulation of CINs, and how they fit into the dysregulation of DA signaling and MSN-mediated control of behavior.

Collectively, the results presented here identify previously unrecognized behavioral roles for long-range VTA GABA projections to CINs, and highlight the functional heterogeneity in their action within the striatum, specifically the NAcSh. These findings broaden our understanding of the diverse roles of both VTA and NAc neuromodulatory interactions, and will aid in our understanding of neuropsychiatric states such as depression and addiction, which directly impact these circuits.

Online content

Any methods, additional references, Nature Research reporting summaries, extended data, supplementary information, acknowledgements, peer review information; details of author contributions

and competing interests; and statements of data and code availability are available at <https://doi.org/10.1038/s41593-021-00898-2>.

Received: 13 December 2019; Accepted: 24 June 2021;
Published online: 12 August 2021

References

- Schultz, W. Dopamine reward prediction-error signalling: a two-component response. *Nat. Rev. Neurosci.* **17**, 183–195 (2016).
- Hamid, A. A. et al. Mesolimbic dopamine signals the value of work. *Nat. Neurosci.* **19**, 117–126 (2016).
- Salamone, J. D. & Correa, M. The mysterious motivational functions of mesolimbic dopamine. *Neuron* **76**, 470–485 (2012).
- Watabe-Uchida, M., Eshel, N. & Uchida, N. Neural circuitry of reward prediction error. *Annu. Rev. Neurosci.* **40**, 373–394 (2017).
- Koob, G. F. & Le Moal, M. Addiction and the brain antireward system. *Annu. Rev. Psychol.* **59**, 29–53 (2008).
- Nestler, E. J. & Carlezon, W. A. Jr. The mesolimbic dopamine reward circuit in depression. *Biol. Psychiatry* **59**, 1151–1159 (2006).
- Ikemoto, S. & Bonci, A. Neurocircuitry of drug reward. *Neuropharmacology* **76**, 329–341 (2014).
- Morales, M. & Margolis, E. B. Ventral tegmental area: cellular heterogeneity, connectivity and behaviour. *Nat. Rev. Neurosci.* **18**, 73–85 (2017).
- Buck, S. A., Torregrossa, M. M., Logan, R. W. & Freyberg, Z. Roles of dopamine and glutamate co-release in the nucleus accumbens in mediating the actions of drugs of abuse. *FEBS J.* **288**, 1462–1474 (2021).
- Creed, M. C., Ntamati, N. R. & Tan, K. R. VTA GABA neurons modulate specific learning behaviors through the control of dopamine and cholinergic systems. *Front. Behav. Neurosci.* **8**, 8 (2014).
- Van Bockstaele, E. J. & Pickel, V. M. GABA-containing neurons in the ventral tegmental area project to the nucleus accumbens in rat brain. *Brain Res.* **682**, 215–221 (1995).
- Brown, M. T. C. et al. Ventral tegmental area GABA projections pause accumbal cholinergic interneurons to enhance associative learning. *Nature* **492**, 452–456 (2012).
- Breton, J. M. et al. Relative contributions and mapping of ventral tegmental area dopamine and GABA neurons by projection target in the rat. *J. Comp. Neurol.* **527**, 916–941 (2019).
- Beier, K. T. et al. Topological organization of ventral tegmental area connectivity revealed by viral-genetic dissection of input–output relations. *Cell Rep.* **26**, 159–167.e6 (2019).
- Lee, J., Finkelstein, J., Choi, J. Y. & Witten, I. B. Linking cholinergic interneurons, synaptic plasticity, and behavior during the extinction of a cocaine–context association. *Neuron* **90**, 1071–1085 (2016).
- Badrinarayan, A. et al. Aversive stimuli differentially modulate real-time dopamine transmission dynamics within the nucleus accumbens core and shell. *J. Neurosci.* **32**, 15779–15790 (2012).
- Al-Hasani, R. et al. Distinct subpopulations of nucleus accumbens dynorphin neurons drive aversion and reward. *Neuron* **87**, 1063–1077 (2015).
- Castro, D. C. & Bruchas, M. R. A motivational and neuropeptidergic hub: anatomical and functional diversity within the nucleus accumbens shell. *Neuron* **102**, 529–552 (2019).
- Reed, S. J. et al. Coordinated reductions in excitatory input to the nucleus accumbens underlie food consumption. *Neuron* **99**, 1260–1273.e4 (2018).
- Castro, D. C. & Berridge, K. C. Opioid hedonic hotspot in nucleus accumbens shell: mu, delta, and kappa maps for enhancement of sweetness ‘liking’ and ‘wanting’. *J. Neurosci.* **34**, 4239–4250 (2014).
- de Jong, J. W. et al. A neural circuit mechanism for encoding aversive stimuli in the mesolimbic dopamine system. *Neuron* **101**, 133–151.e7 (2019).
- Gunaydin, L. A. et al. Natural neural projection dynamics underlying social behavior. *Cell* **157**, 1535–1551 (2014).
- Soden, M. E. et al. Anatomic resolution of neurotransmitter-specific projections to the VTA reveals diversity of GABAergic inputs. *Nat. Neurosci.* **23**, 968–980 (2020).
- Pontieri, F. E., Tanda, G. & Di Chiara, G. Intravenous cocaine, morphine, and amphetamine preferentially increase extracellular dopamine in the ‘shell’ as compared with the ‘core’ of the rat nucleus accumbens. *Proc. Natl Acad. Sci. USA* **92**, 12304–12308 (1995).
- Chen, B. T., Hopf, F. W. & Bonci, A. Synaptic plasticity in the mesolimbic system: therapeutic implications for substance abuse. *Ann. NY Acad. Sci.* **1187**, 129–139 (2010).
- Nestler, E. J. & Aghajanian, G. K. Molecular and cellular basis of addiction. *Science* **278**, 58–63 (1997).
- Hangya, B., Ranade, S. P., Lorenc, M. & Kepecs, A. Central cholinergic neurons are rapidly recruited by reinforcement feedback. *Cell* **162**, 1155–1168 (2015).
- Witten, I. B. et al. Cholinergic interneurons control local circuit activity and cocaine conditioning. *Science* **330**, 1677–1681 (2010).
- Jing, M. et al. An optimized acetylcholine sensor for monitoring in vivo cholinergic activity. *Nat. Methods* **17**, 1139–1146 (2020).
- Klapoetke, N. C. et al. Independent optical excitation of distinct neural populations. *Nat. Methods* **11**, 338–346 (2014).
- Berridge, K. C. & Robinson, T. E. What is the role of dopamine in reward: hedonic impact, reward learning, or incentive salience? *Brain Res. Rev.* **28**, 309–369 (1998).
- van Zessen, R., Phillips, J. L., Budygin, E. A. & Stuber, G. D. Activation of VTA GABA neurons disrupts reward consumption. *Neuron* **73**, 1184–1194 (2012).
- Rizzi, G., Li, Z., Hogrefe, N. & Tan, K. R. Lateral ventral tegmental area GABAergic and glutamatergic modulation of conditioned learning. *Cell Rep.* **34**, 108867 (2021).
- Lowes, D. C. et al. Ventral tegmental area GABA neurons mediate stress-induced blunted reward-seeking in mice. *Nat. Commun.* **12**, 1–13 (2021).
- Aosaki, T. et al. Responses of tonically active neurons in the primate striatum undergo systematic changes during behavioral sensorimotor conditioning. *J. Neurosci.* **14**, 3969–3984 (1994).
- Apicella, P. Leading tonically active neurons of the striatum from reward detection to context recognition. *Trends Neurosci.* **30**, 299–306 (2007).
- Collins, A. L. & Saunders, B. T. Heterogeneity in striatal dopamine circuits: form and function in dynamic reward seeking. *J. Neurosci. Res.* **98**, 1046–1069 (2020).
- Shin, J. H., Adrover, M. F., Wess, J. & Alvarez, V. A. Muscarinic regulation of dopamine and glutamate transmission in the nucleus accumbens. *Proc. Natl Acad. Sci. USA* **112**, 8124–8129 (2015).
- Dorst, M. C. et al. Polysynaptic inhibition between striatal cholinergic interneurons shapes their network activity patterns in a dopamine-dependent manner. *Nat. Commun.* **11**, 5113 (2020).
- Lewis, R. G. et al. Dopaminergic control of striatal cholinergic interneurons underlies cocaine-induced psychostimulation. *Cell Rep.* **31**, 107527 (2020).
- Shin, J. H., Adrover, M. F. & Alvarez, V. A. Distinctive modulation of dopamine release in the nucleus accumbens shell mediated by dopamine and acetylcholine receptors. *J. Neurosci.* **37**, 11166–11180 (2017).
- Chuhma, N., Mingote, S., Moore, H. & Rayport, S. Dopamine neurons control striatal cholinergic neurons via regionally heterogeneous dopamine and glutamate signaling. *Neuron* **81**, 901–912 (2014).
- Zhang, Y.-F. & Cragg, S. J. Pauses in striatal cholinergic interneurons: what is revealed by their common themes and variations? *Front. Syst. Neurosci.* **11**, 80 (2017).
- Crespo, J. A., Stöckl, P., Zorn, K., Saria, A. & Zernig, G. Nucleus accumbens core acetylcholine is preferentially activated during acquisition of drug- vs food-reinforced behavior. *Neuropsychopharmacology* **33**, 3213–3220 (2008).
- Aitta-aho, T. et al. Accumbal cholinergic interneurons differentially influence motivation related to satiety signaling. *eNeuro* <https://doi.org/10.1523/ENEURO.0328-16.2017> (2017).
- Pratt, W. E. & Kelley, A. E. Nucleus accumbens acetylcholine regulates appetitive learning and motivation for food via activation of muscarinic receptors. *Behav. Neurosci.* **118**, 730–739 (2004).
- Nougaret, S. & Ravel, S. Modulation of tonically active neurons of the monkey striatum by events carrying different force and reward information. *J. Neurosci.* **35**, 15214–15226 (2015).
- Collins, A. L. et al. Dynamic mesolimbic dopamine signaling during action sequence learning and expectation violation. *Sci. Rep.* **6**, 20231 (2016).
- Cachope, R. et al. Selective activation of cholinergic interneurons enhances accumbal phasic dopamine release: setting the tone for reward processing. *Cell Rep.* **2**, 33–41 (2012).
- London, T. D. et al. Coordinated ramping of dorsal striatal pathways preceding food approach and consumption. *J. Neurosci.* **38**, 3547–3558 (2018).
- Threlfell, S. et al. Striatal dopamine release is triggered by synchronized activity in cholinergic interneurons. *Neuron* **75**, 58–64 (2012).
- Piccio, M. R., Higley, M. J. & Mineur, Y. S. Acetylcholine as a neuromodulator: cholinergic signaling shapes nervous system function and behavior. *Neuron* **76**, 116–129 (2012).
- Dautan, D. et al. A major external source of cholinergic innervation of the striatum and nucleus accumbens originates in the brainstem. *J. Neurosci.* **34**, 4509–4518 (2014).
- Tashakori-Sabzevar, F. & Ward, R. D. Basal forebrain mediates motivational recruitment of attention by reward-associated cues. *Front. Neurosci.* **12**, 786 (2018).
- Ballinger, E., Ananth, M., Talmage, D. A. & Role, L. Basal forebrain cholinergic circuits and signaling in cognition and cognitive decline. *Neuron* **91**, 1199–1218 (2016).
- Koob, G. F. & Volkow, N. D. Neurocircuitry of addiction. *Neuropsychopharmacology* **35**, 217–238 (2010).
- Saunders, B. T. & Janak, P. H. Nucleus accumbens plasticity underlies multifaceted behavioral changes associated with addiction. *Biol. Psychiatry* **75**, 92–93 (2014).

58. Scofield, M. D. et al. The nucleus accumbens: mechanisms of addiction across drug classes reflect the importance of glutamate homeostasis. *Pharm. Rev.* **68**, 816–871 (2016).
59. Di Chiara, G. Nucleus accumbens shell and core dopamine: differential role in behavior and addiction. *Behav. Brain Res* **137**, 75–114 (2002).
60. Hikida, T., Kitabatake, Y., Pastan, I. & Nakanishi, S. Acetylcholine enhancement in the nucleus accumbens prevents addictive behaviors of cocaine and morphine. *Proc. Natl Acad. Sci. USA* **100**, 6169–6173 (2003).
61. Gonzales, K. K. & Smith, Y. Cholinergic interneurons in the dorsal and ventral striatum: anatomical and functional considerations in normal and diseased conditions. *Ann. NY Acad. Sci.* **1349**, 1–45 (2015).
62. Warner-Schmidt, J. L. et al. Cholinergic interneurons in the nucleus accumbens regulate depression-like behavior. *Proc. Natl Acad. Sci. USA* **109**, 11360–11365 (2012).
63. Cheng, J., Umschweif, G., Leung, J., Sagi, Y. & Greengard, P. HCN2 channels in cholinergic interneurons of nucleus accumbens shell regulate depressive behaviors. *Neuron* **101**, 662–672.e5 (2019).

Publisher's note Springer Nature remains neutral with regard to jurisdictional claims in published maps and institutional affiliations.

© The Author(s), under exclusive licence to Springer Nature America, Inc. 2021

Methods

Experimental subjects. For all experiments adult (25–35 g), 12- to 16-week-old, VGAT-Cre, ChAT-Cre or WT C57BL-6 male and female mice were group housed, given free access to food pellets, and maintained on a 12 h:12 h light:dark cycle (lights on at 07:00). All animals were kept in a sound-attenuated, isolated housing facility in the lab 1 week before surgery, post-surgery and throughout the duration of the behavioral assays to minimize stress. All procedures were approved by the Institute of Animal Care and Use Committee (IACUC) of Washington University in St. Louis and the IACUC of the University of Washington, and conformed to US National Institutes of Health guidelines. All studies were performed in compliance with IACUC ethical guidelines.

Animals were randomly assigned to experimental groups and stimulus presentation. All experiments were replicated in at least one additional independent group. Experimenters were also blinded to the experimental groups for all experiments. The *n* numbers were 5–11 mice per experiment/experimental group, across all experiments. Exact animal numbers are provided in the legends for each figure. Animals were excluded only after post-hoc validation for virus expression and/or fiber placements.

Stereotaxic surgery. Mice were anesthetized in an induction chamber (2–4% isoflurane) and placed into a stereotaxic frame (Kopf Instruments, Model 1900) where they were maintained at 1–2% isoflurane. Male and female mice were anesthetized, after which we performed a craniotomy and unilaterally injected, using a blunt neural syringe (Hamilton Company, catalog no. 65457-01), 300–400 nl of AAVDJ-DIO-GCaMP6s (Stanford Viral Vector Core, viral titer $1-2 \times 10^{13}$ vector genomes (vg) ml⁻¹), AAV9-GRAB-ACh3.0 (WZ Bioscience, viral titer $1-2 \times 10^{13}$ vg ml⁻¹), AAV5-DIO-ChR2-eYFP, AAV5-DIO-ChrimsonR-tdTomato (Hope Center Viral Vector Core, viral titer 5×10^{12} vg ml⁻¹) or AAV5-DIO-eYFP (Hope Center Viral Vector Core, viral titer 2×10^{13} vg ml⁻¹) into the VTA (stereotaxic coordinates from Bregma: -3.15 to -3.4 mm AP, ± 0.5 mm mediolateral (ML), -4.5 to 4.75 mm dorsoventral (DV)), followed by optic fiber implantation 5 weeks later into the vNacSh (stereotaxic coordinates from Bregma: +1.3 mm (AP), ± 0.5 mm (ML), -4.2 mm (DV)), vNacSh (stereotaxic coordinates from Bregma: +1.3 mm (AP), ± 0.5 mm (ML), -4.7 mm (DV)) or NAcC (stereotaxic coordinates from Bregma: +1.0 mm (AP), ± 1.0 mm (ML), -4.7 mm (DV))⁶⁴. For the ChAT-Cre ChR2 or GCaMP6s experiments, the vNacSh coordinates listed above were used to inject 300 nl of AAV5-DIO-ChR2-eYFP or AAV5-DIO-eYFP or AAVDJ-DIO-GCaMP6s immediately followed by optic fiber implantation. For the ChAT-Cre enhanced NpHR (eNpHR) experiments, we bilaterally injected, using a blunt neural syringe, 300 nl of AAV5-DIO-eNpHR-eYFP into the vNacSh at an 8° angle (stereotaxic coordinates from Bregma: +1.3 mm (AP), ± 1.17 mm (ML), -4.80 mm (DV)). For the JAWS experiments, we bilaterally injected, using a blunt neural syringe, 300 nl of AAV5-DIO-JAWS-eYFP into the VTA and implanted optic fibers into the vNacSh at an 8° angle (stereotaxic coordinates from Bregma: +1.3 mm (AP), ± 1.17 mm (ML), -4.80 mm (DV)). We secured the implants using two bone screws and a dental cement head cap (Lang Dental).

Fiber photometry. For fiber photometry studies, mice were initially food deprived to 90% of their body weight and trained in a pavlovian and then an operant behavioral paradigm with a modular test chamber (17.8 × 15.2 × 18.4 cm³; Med Associates Inc.). Fiber photometry recordings were made throughout the entirety of 30-min pavlovian conditioning and operant training sessions as previously described⁶⁵. Before recording during pavlovian or operant behavior sessions, an optic fiber was attached to the implanted fiber using a ferrule sleeve (Doric, catalog no. ZR_2.5). Two light-emitting diodes (LEDs) were used to excite GCaMP6s. A 531-Hz sinusoidal LED light (Thorlabs, LED light, catalog no. M470F3; LED driver, catalog no. DC4104) was bandpass filtered (470 ± 20 nm, Doric, catalog no. FMC4) to excite GCaMP6s and evoke Ca²⁺-dependent emission. A 211-Hz sinusoidal LED light (Thorlabs, LED light, catalog no. M405FP1; LED driver, catalog no. DC4104) was bandpass filtered (405 ± 10 nm, Doric, catalog no. FMC4) to excite GCaMP6s and evoke Ca²⁺-independent isosbestic control emission. Laser intensity for the 470-nm and 405-nm wavelength bands was measured at the tip of the optic fiber and adjusted to 50 μW before each day of recording. GCaMP6s fluorescence traveled through the same optic fiber before being bandpass filtered (525 ± 25 nm, Doric, catalog no. FMC4), transduced by a femtowatt silicon photoreceiver (Newport, catalog no. 2151) and recorded by a real-time processor (TDT, catalog no. RZ5P). The envelopes of the 531-Hz and 211-Hz signals were extracted in real time by the TDT program Synapse at a sampling rate of 1,017.25 Hz. For the ChrimsonR stimulation experiments, a 625-nm laser was used at 3- to 5-mW intensity to deliver red light through the tip of the same optic fiber used to excite GCaMP6s.

Pavlovian behavior paradigm (photometry). The mice freely roamed in an operant chamber in which there was a house light and pellet receptacle. The house light illuminated as the conditioned stimulus (CS) and sucrose pellets (20 mg, BioServe) were the unconditioned stimulus (US). The trial consisted of 18 s of CS presentation and a single sucrose pellet was dropped 6 s after CS onset. The ITI was randomized between 70 and 100 s. A total session was 30 min. On pavlovian training day 7, the animal received only CS (US omitted) in the session.

Operant behavior paradigm (photometry). The mice freely roamed in an operant chamber in which there was a house light, pellet receptacle and two nosepoke ports. The house light illuminated as the CS and sucrose pellets (20 mg) were the US. Meeting the nosepoke criterion (FR-1 or FR-3) began 12 s of CS presentation and a single sucrose pellet was dropped 6 s after CS onset. Any additional, redundant nosepoking during the CS period was not counted. A total session was 30 min. On operant training day 7, the animal received only CS (US omitted) for the session.

Photometry analysis. Customized MatLab scripts were developed for analyzing fiber photometry data in the context of mouse behavior. The isosbestic 405-nm excitation control signal was subtracted from the 470-nm excitation signal to remove movement artifacts from intracellular, Ca²⁺-dependent, GCaMP6s fluorescence. Baseline drift was evident in the signal due to slow photobleaching artifacts, particularly during the first few minutes of each 30-min recording session. A double exponential curve was fit to the raw trace and subtracted to correct for baseline drift. After baseline correction, the photometry trace was z-scored relative to the mean and s.d. of the 30-min session. The post-processed fiber photometry signal was analyzed in the context of animal behavior during pavlovian conditioning and operant task performance. Pearson's correlations, one-sample Student's *t*-tests, two-sample Student's *t*-tests and two-way analysis of variance (ANOVA) were performed using standard MatLab functions 'corr', 'ttest', 'ttest2' and 'anovan', respectively. Peak, mean and minimum fluorescence were determined during predetermined time windows for the cue period (0–6 s) and reward period (6–30 s), and subtracted from peak, mean or minimum fluorescence values in a baseline window (-10 to 0 s; -10 to 5 s for nosepoke 'ramp' determinations). Code that supports the analysis will be made available from the corresponding author upon reasonable request.

Real-time place testing. All behaviors were performed within a sound-attenuated room maintained at 23 °C at least 1 week after habituation to the holding room and the final surgery. Lighting was stabilized at 1,500 lux. Movements were video recorded and analyzed using Ethovision XT 10.0 (Noldus Information Technologies). For real-time place testing, after recovery from surgery (please refer to Stereotaxic surgery for further information on procedure) mice were gently placed in a customized, unbiased, balanced, two-compartment conditioning apparatus (52.5 × 25.5 × 25.5 cm³) as described previously^{17,66,67}. During a 20-min trial, entry into one compartment triggered photostimulation (10-ms pulse width) of various frequencies (2, 5, 10, 15, 20, 40, 60 Hz, and so on), whereas the animal remained in the light-paired chamber and entry into the other chamber ended photostimulation. The experimental animals were counterbalanced for both group and stimulation side. Preference scores in each experiment were determined by computing the percentage of time spent in the 'light stimulation' side out of the total explored time during the tests. All behavioral data, including traveled distance and time, were collected and analyzed using Ethovision v.9.5 software (Noldus Information Technologies, catalog no. RRID:SCR_000441) with a digital camera (Canon, catalog no. ZR900) mounted above.

Operant self-stimulation. All tests took place in mouse operant chambers (17.8 × 15.2 × 18.4 cm³; Med Associates). A rotating optical commutator (Doric) was located on the top of the operant chamber and connected to a 473-nm, diode-pumped, solid-state laser (OEM Laser Systems; see Fig. 2f). Fibers were connected to the implants on the mouse for every training session. The conditioning chamber light was turned on during every training session. Laser power was adjusted to obtain ~10 mW transmittance into the brain. Mice were trained to nosepoke in a Med Associates' operant box with two nosepoke portals available: 'active' and 'inactive'. Successful nosepokes on the active nosepoker rewarded the mouse with 2 s of stimulation (40 Hz, 10-ms pulse width). An orange cue light turned on above the sipper during the 2-s stimulation period. Nosepoking to the inactive portal produced no consequences or rewards. Once discrimination was acquired over 1-h-long FR-1 sessions (<30% of total poking in the inactive hole), mice underwent one session of FR-3. Mice's motivation was then assessed using a 1-h session of progressive ratio schedule of reinforcement. The data were calculated as the total number of nosepokes at the active and inactive sites for each day over the course of the experiment^{17,65}.

Uncued reward delivery. All tests took place in mouse operant chambers (17.8 × 15.2 × 18.4 cm³; Med Associates). A rotating optical commutator (Doric) was located on the top of the operant chamber and connected to a 625-nm, diode-pumped, solid-state laser (for JAWS experiments) or 473-nm, diode-pumped, solid-state laser (OEM Laser Systems; see Fig. 2f). Fibers were connected to the implants on the mouse for every training session. Sucrose pellets were delivered at a variable ITI (VI-90s) and animal head entries were recorded by outfitting the pellet receptacles with customized infrared sensors to record beam breaks during head entries. On training, animals underwent counterbalanced laser on versus off sessions, where the laser was delivered for 10 s either side of reward delivery. Laser power was adjusted to obtain ~5 mW transmittance into the brain for JAWS experiments and ~10 mW transmittance for ChR2 experiments. For the JAWS experiments, we used previously employed parameters for laser delivery: 2 s

on, 2 s ramp down and 2 s off. For Chr2 experiments, we used 20 Hz, 5-ms pulse width for laser delivery.

Immunohistochemistry and quantification. At the end of each study, animals were perfused with 4% paraformaldehyde followed by anatomic analysis to confirm injection sites and cell-type-specific expression. For animals used in Fig. 3, a ChAT stain (MilleporeSigma, catalog no. ab144p, 1:500 dilution) and anti-green fluorescent protein (Abcam, catalog no. ab13970, 1:2,000 dilution) was used to identify the VTA where Chr2 was injected. Immunohistochemistry and quantification were performed as previously described^{17,66,68}.

Electrophysiology. Coronal ex vivo slices (240 μ m) containing NAcC and NAcSh were prepared as described previously from *VGAT-cre** mice injected with Chr2. Cutting solution consisted of the following (in mM): 225 sucrose, 13.9 NaCl, 26.2 NaHCO₃, 1 NaH₂PO₄, 1.25 glucose, 2.5 KCl, 0.1 CaCl₂, 4.9 MgCl₂ and 3 kynurenic acid. Slices were maintained in oxygenated artificial cerebrospinal fluid containing (in mM): 124 NaCl, 2.5 KCl, 2.5 CaCl₂, 1.3 MgCl₂, 26.2 NaHCO₃, 1 NaH₂PO₄ and 20 glucose (~310–315 mosmol) at room temperature after a 1-h recovery period at 33 °C. CINs were identified in situ by the size of their soma and spontaneous firing pattern. Non-CINs/putative MSNs were presumed based on soma size, membrane resistance (100–500 M Ω), lack of spontaneous activity and hyperpolarized resting membrane potential. We used two different internal solutions (in mM): 60 CsMeSO₃, 60 CsCl, 10 4-(2-hydroxyethyl)-1-piperazine-ethanesulfonic acid (Hepes), 0.2 (ethylenebis(oxonitrilo))tetra-acetate (EGTA), 8 NaCl, 2 MgCl₂, 2 Mg ATP, 0.3 Na GTP and 10 phosphocreatine, pH 7.24 (~300 mosmol) or 70 KMeSO₃, 70 KCl, 10 Hepes, 0.2 K EGTA, 2 MgCl₂, 4 Na ATP, 0.4 Na GTP, 10 phosphocreatine, pH 7.25 (~290 mosmol). Cells were excluded in instances where the access resistance exceeded \pm 25% of the baseline recording. We used the cesium-based internal solution at first to allow for better space clamping; however, we found that this was suboptimal for consistent detection of spontaneous firing in cell-attached mode. We, therefore, switched to a potassium-based solution so that we could better identify spontaneously active versus nonspontaneously active neurons. As there were no significant differences in oIPSC amplitude in putative CINs or MSNs between the two internal solutions, we were able to combine data collected using them. In a subset of experiments, the internal solution contained biocytin. The cells were filled with biocytin whereas the internal solution was used to dialyze the cell. After the end of the experiment, slices were fixed and kept for subsequent immunohistochemistry. Immunohistochemistry for ChAT-ir (immunoreactive) and biocytin was conducted on slices using standard procedures. This was done to confirm the identity of the CINs. Data were acquired using pClamp 10 and analyzed using Clampfit 10 (Molecular Devices) and MiniAnalysis (Synaptosoft).

Statistics and reproducibility. Before starting the studies, power analyses to determine sample sizes and detect differences between groups were calculated using G*Power 3. For these calculations, effect sizes estimated from published data or, in some cases, from small pilot studies were run for this purpose. For all data, D'Agostino–Pearson normality tests were performed, and nonparametric analyses were used for any ordinal or not normally distributed data. For all studies data were expressed as mean \pm s.e.m. Statistical significance was taken as * P < 0.05, ** P < 0.01, *** P < 0.001 and **** P < 0.0001, as determined by a Student's t -test, one-way ANOVA or a two-way, repeated-measure ANOVA, followed by post-hoc tests as appropriate. GraphPad Prism and MatLab were used for data analysis and statistical comparisons. All experiments were replicated in at least one additional independent group.

Reporting Summary. Further information on research design is available in the Nature Research Reporting Summary linked to this article.

Data availability

The raw data that support the findings of the present study are available from the corresponding authors upon request.

Code availability

Custom MATLAB code used for data analysis is available at <https://github.com/BruchasLab>.

References

- Sparta, D. R. et al. Construction of implantable optical fibers for long-term optogenetic manipulation of neural circuits. *Nat. Protoc.* **7**, 12–23 (2012).
- Parker, K. E. et al. A paranigral VTA nociceptin circuit that constrains motivation for reward. *Cell* **178**, 653–671.e19 (2019).
- McCall, J. G. et al. CRH engagement of the locus coeruleus noradrenergic system mediates stress-induced anxiety. *Neuron* **87**, 605–620 (2015).
- Siuda, E. R. et al. Spatiotemporal control of opioid signaling and behavior. *Neuron* **86**, 923–935 (2015).
- Kim, T. et al. Injectable, cellular-scale optoelectronics with applications for wireless optogenetics. *Science* **340**, 211–216 (2013).

Acknowledgements

We thank all at M.R.B.'s lab and R.A.H.'s lab, and J. McCall for their helpful insight and discussion throughout the preparation of the manuscript, and in particular C. Stander, L. Lawson, D. Blumenthal and A. Suko for their technical support. We thank our funding sources: NIH/NIDA K99/R00 DA038725 (to R.A.-H.), NIH/NIDA F31 DA051124 (to C.E.P.), Addictions, Drug and Alcohol Institute (ADAI) Fellowship (to D.J.M.), SCAN Design Fellowship (to S.E.S.), Mary Gates Fellowship (to A.E.J.), NIH/NIMH K99/R00 MH109627 (to J.C.L.) and NIH/NIDA R37 DA033396, P30 DA048736 (to M.R.B.).

Author contributions

R.A.-H., G.P.S., R.G. and M.R.B. conceptualized and designed the experiments. R.A.-H., R.G., G.P.S., T.E.H., S.E.S., A.J.E. and J.C.L. performed the surgeries. J.C.L. and D.J.M. performed the electrophysiology. R.G., S.E.S. and C.E.P. performed the fiber photometry. R.G. and C.E.P. recorded the ITI. R.A.-H., R.G., A.J.E., T.E.H., G.P.S. and J.C.L. carried out the immunohistochemistry. R.G. did the uncued reward delivery. R.A.-H., R.G. and G.P.S. performed the operant self-stimulation and real-time place testing. R.G., C.E.P. and S.E.S. carried out the operant behavior paradigm (photometry) and the pavlovian behavior paradigm (photometry). Y.L. and M.J. provided the sensor resources. R.A.-H., R.G., G.P.S., C.E.P., J.C.L., V.A.A. and M.R.B. wrote the original draft, and reviewed and edited it. R.A.-H. and M.R.B. acquired funds. R.A.-H. and M.R.B. administered the project.

Competing interests

The authors declare no competing interests.

Additional information

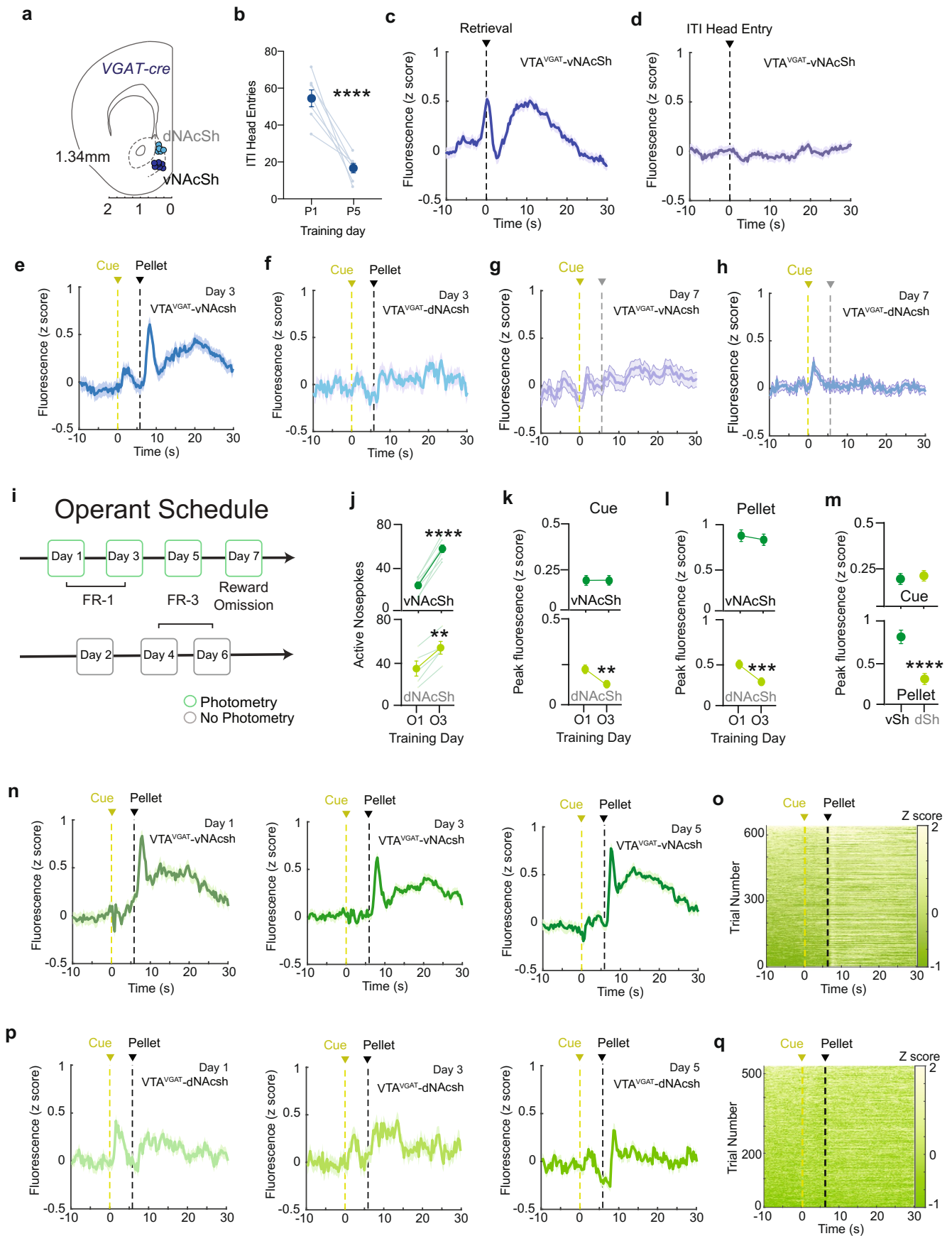
Extended data are available for this paper at <https://doi.org/10.1038/s41593-021-00898-2>.

Supplementary information The online version contains supplementary material available at <https://doi.org/10.1038/s41593-021-00898-2>.

Correspondence and requests for materials should be addressed to R.A.-H. or M.R.B.

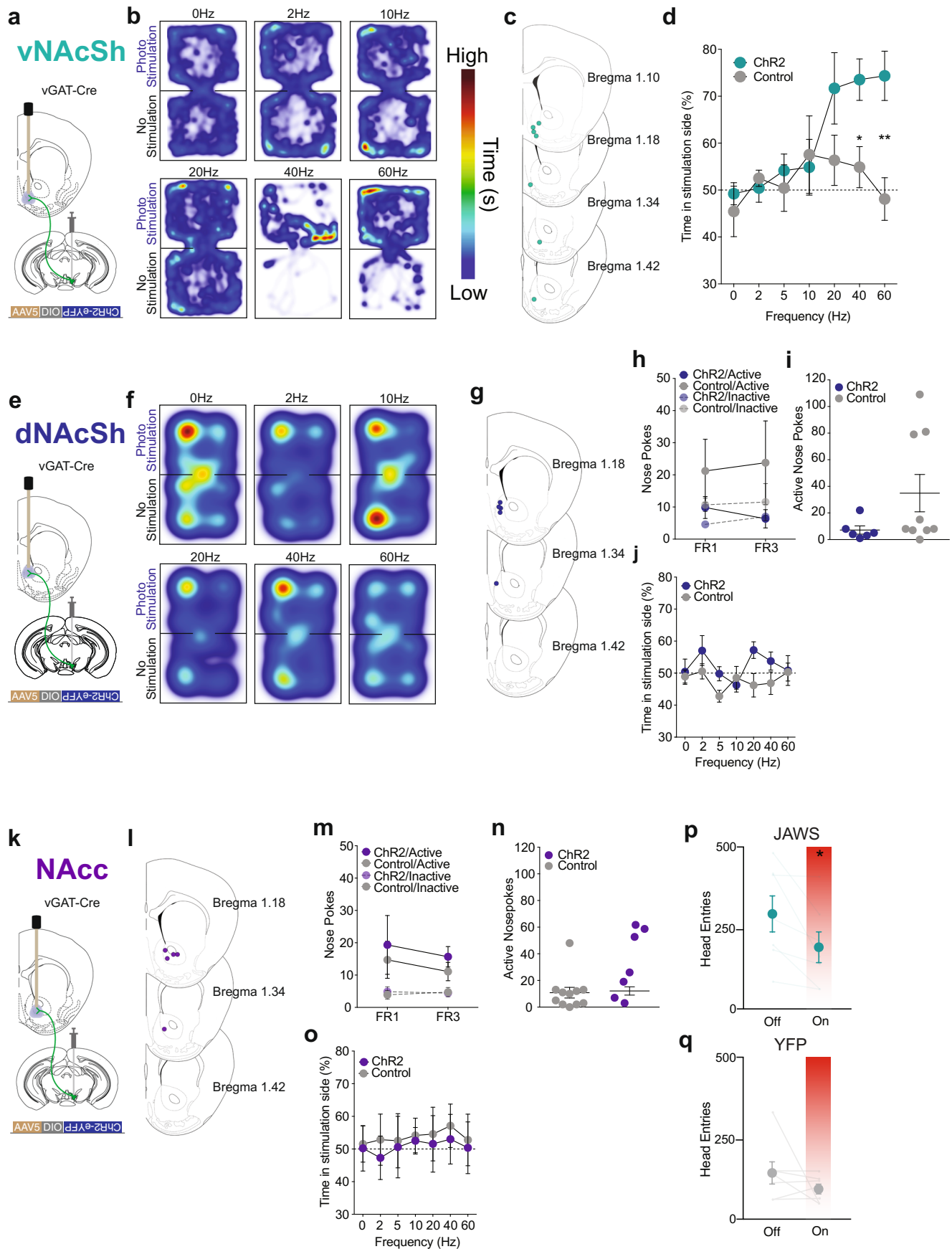
Peer review information *Nature Neuroscience* thanks William Howe and the other, anonymous, reviewer(s) for their contribution to the peer review of this work.

Reprints and permissions information is available at www.nature.com/reprints.



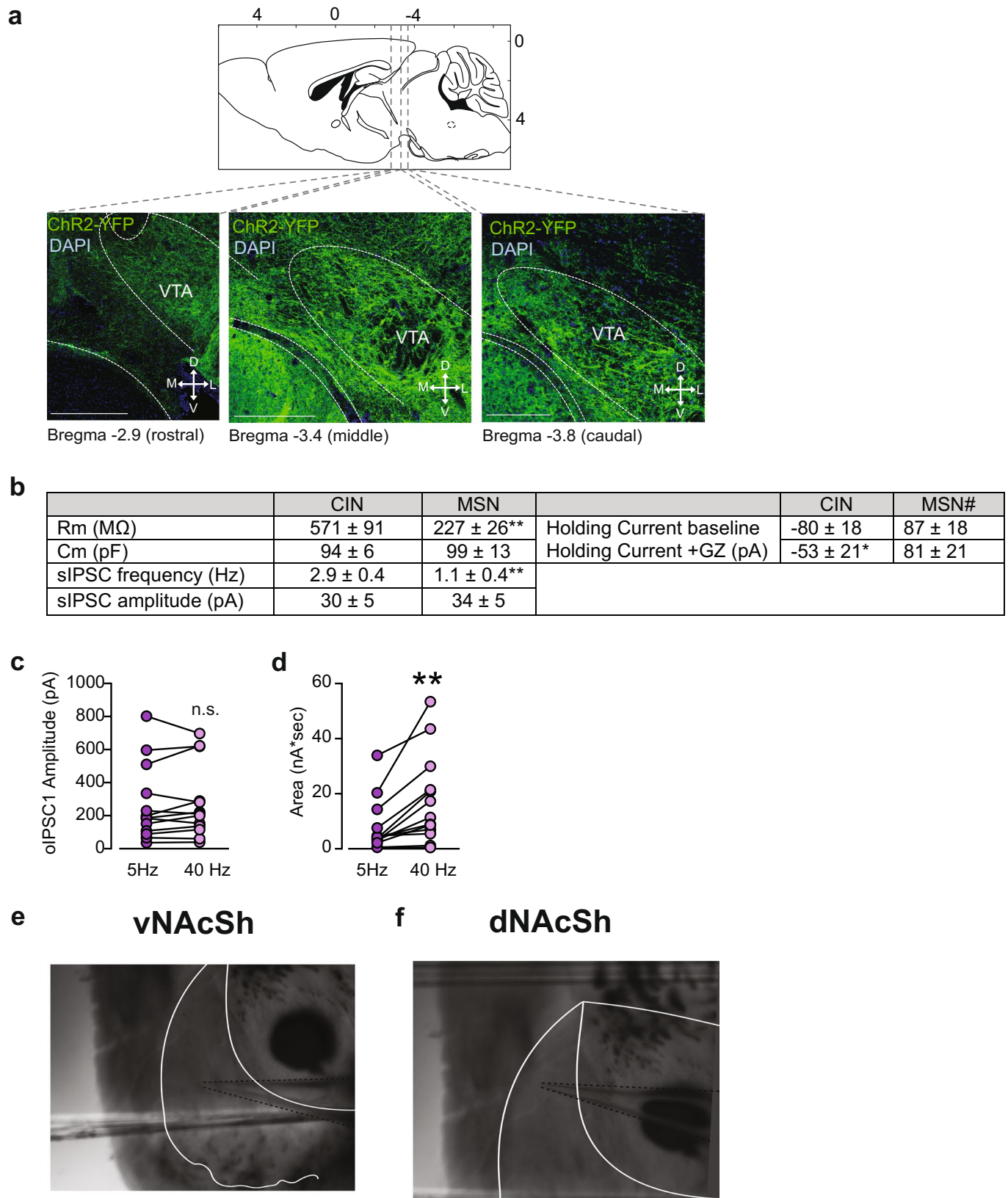
Extended Data Fig. 1 | See next page for caption.

Extended Data Fig. 1 | VTA GABAergic terminals in the vNAcSh are preferentially engaged during reward reinforcement. (a) Coronal brain cartoon of fiber placements in the dNAcSh (light blue; $n=5$) or vNAcSh (dark blue; $n=7$) of VGAT-Cre+ mice. (b) Inter-trial interval (ITI) head entries for Pavlovian training, vNAcSh ($n=7$ mice; P1 vs. P5 paired t test $p=0.0008$, $t=6.274$, $df=6$). (c) Mean vNAcSh recorded calcium activity during pellet retrieval averaged across all trials from day 1-5 of Pavlovian conditioning ($n=7$ mice). Data represented as mean \pm SEM. (d) Mean vNAcSh recorded calcium activity during unrewarded, ITI head entries averaged across all trials from day 1-5 of Pavlovian conditioning ($n=7$ mice). Data represented as mean \pm SEM. (e) Mean vNAcSh recorded calcium activity averaged across all trials from day 3 of Pavlovian conditioning ($n=7$ mice). Data represented as mean \pm SEM. (f) Mean dNAcSh recorded calcium activity averaged across all trials from day 3 of Pavlovian conditioning ($n=5$ mice). Data represented as mean \pm SEM. (g) Mean vNAcSh recorded calcium activity averaged across all trials from day 7 of Pavlovian conditioning extinction ($n=7$ mice). Data represented as mean \pm SEM. (h) Mean dNAcSh recorded calcium activity averaged across all trials from day 7 of Pavlovian conditioning extinction ($n=5$ mice). Data represented as mean \pm SEM. (i) Operant training schedule with photometry recordings, as indicated. (j) Top - vNAcSh active nosepekes for Operant training days ($n=7$ mice; O1 vs. O3 paired t test $p>0.0001$, $t=14.24$, $df=6$). Bottom - dNAcSh active nosepekes for Operant training days ($n=5$ mice; O1 vs. O3 paired t test $p=0.0035$, $t=6.180$, $df=4$). Data represented as mean \pm SEM. (k) Peak fluorescence during cue period (0-6 s) for Operant training days. Top - vNAcSh ($n=7$ mice; O1 vs. O3 paired t test $p=0.5002$, $t=0.6759$, $df=142$). Bottom - dNAcSh ($n=5$ mice; O1 vs. O3 paired t test $p=0.0047$, $t=2.871$, $df=146$). Data represented as mean \pm SEM. (l) Peak fluorescence during reward period (6-30 s) for Operant training days. Top - vNAcSh ($n=7$ mice; O1 vs. O3 paired t test $p=0.9724$, $t=0.3463$, $df=141$). Bottom - dNAcSh ($n=5$ mice; O1 vs. O3 vs. P5 paired t test $p=0.0003$, $t=3.702$, $df=146$). Data represented as mean \pm SEM. (m) Top - Peak fluorescence during cue period (0-6 s) comparing vNAcsh ($n=7$ mice) vs. dNAcSh ($n=5$ mice) for Operant training (unpaired t test, $p=0.6729$, $t=0.4222$, $df=1038$). Bottom - Peak fluorescence during reward period (6-30 s) comparing vNAcsh vs. dNAcSh for Operant training (unpaired t test, $p<0.0001$, $t=9.513$, $df=1038$). Data represented as mean \pm SEM. (n) Mean vNAcSh recorded calcium activity averaged across all trials from day 1-5 of Operant conditioning ($n=7$ mice). Data represented as mean \pm SEM. (o) Heatmap raster plot of vNAcSh recorded calcium activity for every trial of Operant conditioning across all days. Trials are displayed in ascending order by average activity following pellet delivery ($n=7$ mice). (p) Mean dNAcSh recorded calcium activity averaged across all trials from day 1-5 of Operant conditioning ($n=5$ mice). Data represented as mean \pm SEM. (q) Heatmap raster plot of vNAcSh recorded calcium activity for every trial of Operant conditioning across all days. Trials are displayed in ascending order by average activity following pellet delivery ($n=5$ mice).



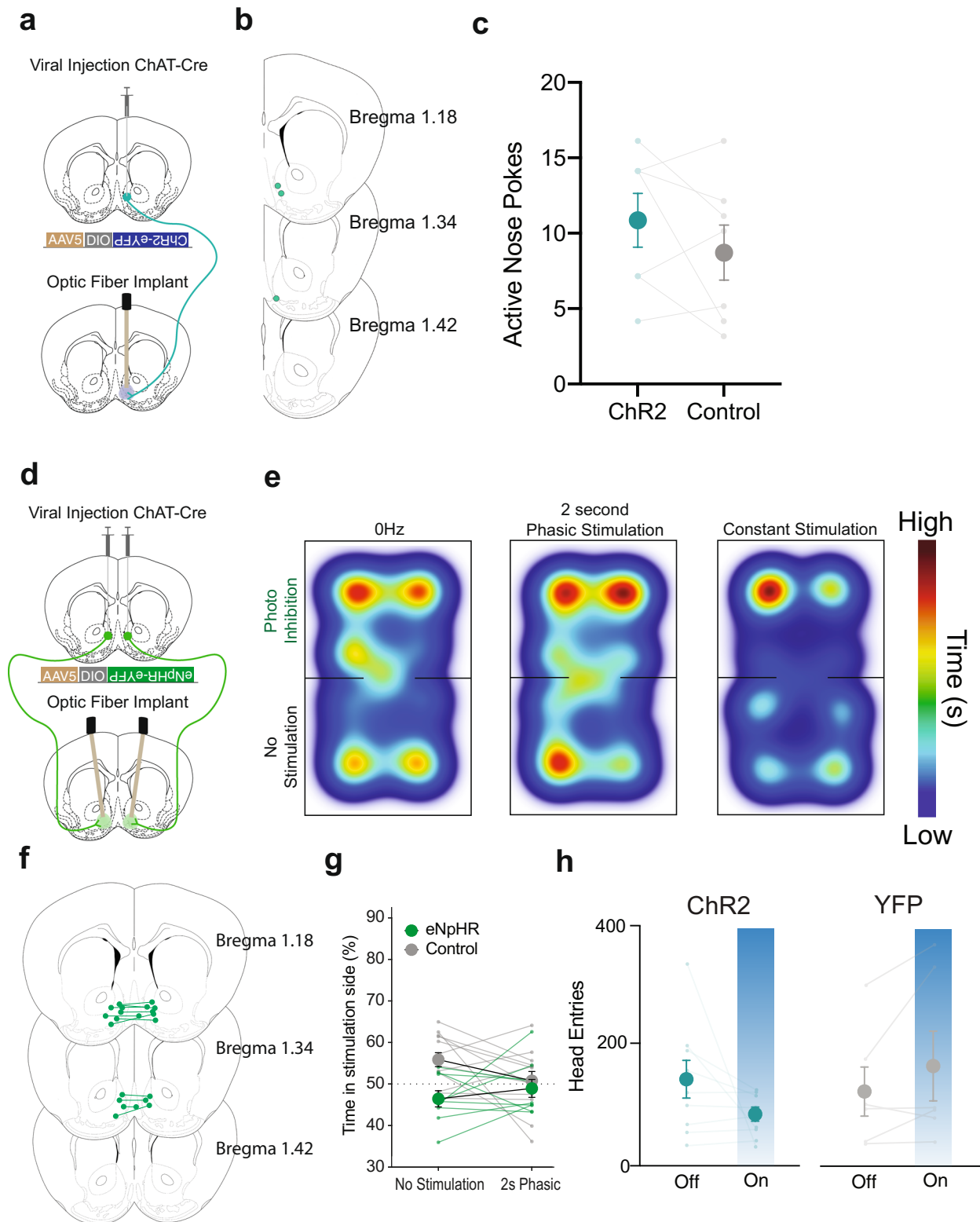
Extended Data Fig. 2 | See next page for caption.

Extended Data Fig. 2 | Photo-activation of VTA GABAergic projections to the vNAcSh promotes positive reinforcement. (a) Cartoon of ventral NAcSh fiber optic placement. (b) Representative examples of real-time mouse heatmap raster plots following no stimulation, 2 Hz, 10 Hz, 20 Hz, 40 Hz, and 60 Hz ventral NAcSh photostimulation. (c) Hit map showing fiber optic placements of each individual mouse included in the ventral NAcSh Chr2 group. (d) Frequency response curve showing photostimulation of vGAT terminal in vNAcSh at no stimulation, 2 Hz, 5 Hz, 10 Hz, 20 Hz, 40 Hz, and 60 Hz; 20 ms pulse width. Photostimulation shows significant preference at 40 and 60 Hz. Unpaired Student's t Test, two-tailed, Control vs Chr2, $*p < 0.05$; Unpaired Student's t Test, two-tailed, Chr2 group 0 vs 40 Hz, $**p < 0.01$ (data represented as mean \pm SEM, $n = 6$ mice/Control, 7 mice/Chr2). (e) Cartoon of dorsal NAcSh fiber optic placement. (f) Representative examples of real-time mouse heatmap raster plots following no stimulation, 2 Hz, 10 Hz, 20 Hz, 40 Hz, and 60 Hz dorsal NAcSh photostimulation. (g) Hit map showing fiber optic placements of each individual mouse included in the dorsal NAcSh Chr2 group. (h) Data showing number of nose pokes during fixed-ratio 1 testing versus fixed-ratio 3 testing (data represented as mean \pm SEM, $n = 6$ mice/FR-3, 9 mice/FR-1). (i) Data showing number of nose pokes during progressive ratio testing with no significant differences between control and experimental groups ((data represented as mean \pm SEM, $n = 6$ mice/Control, 9 mice/Experimental). (j) Frequency response curve showing photostimulation of vGAT terminal in dNAcSh at no stimulation, 2 Hz, 5 Hz, 10 Hz, 20 Hz, 40 Hz, and 60 Hz; 20 ms pulse width. Photostimulation shows no significant preference. Control vs Chr2 (data represented as mean \pm SEM, $n = 6$ mice/Control, $n = 10$ mice/Chr2). (k) Cartoon of NAcc fiber optic placement. (l) Hit map showing fiber optic placements of each individual mouse included in the NAcc Chr2 group. (m) Data showing number of nose pokes during fixed-ratio 1 testing versus fixed-ratio 3 testing (data represented as mean \pm SEM, $n = 7$ mice/FR-3, 11 mice/FR-1). (n) Data showing number of nose pokes during progressive ratio testing with no significant differences between control and experimental groups ((data represented as mean \pm SEM, $n = 7$ mice/Control, 11 mice/Experimental). (o) Frequency response curve showing photostimulation of vGAT terminal in NAcc at no stimulation, 2 Hz, 5 Hz, 10 Hz, 20 Hz, 40 Hz, and 60 Hz; 20 ms pulse width. Photostimulation shows no significant preference. Control vs Chr2 (data represented as mean \pm SEM, $n = 6$ mice/Control, 8 mice/Chr2). (p) Total head entries performed in matched, counterbalanced sessions comparing laser on vs. off (pulse – 2 s on, 2 s ramp down, 1 s off) in the JAWS group ($n = 7$ mice; Off vs. On paired t test $p = 0.0269$, $t = 2.913$, $df = 6$). Right - YFP group ($n = 7$ mice; Off vs. On paired t test $p = 0.2739$, $t = 1.204$, $df = 6$). Data represented as mean \pm SEM. (q) Total head entries performed in matched, counterbalanced sessions comparing laser on vs. off (pulse – 2 s on, 2 s ramp down, 1 s off) in the YFP group ($n = 7$ mice; Off vs. On paired t test $p = 0.2739$, $t = 1.204$, $df = 6$). Data represented as mean \pm SEM.



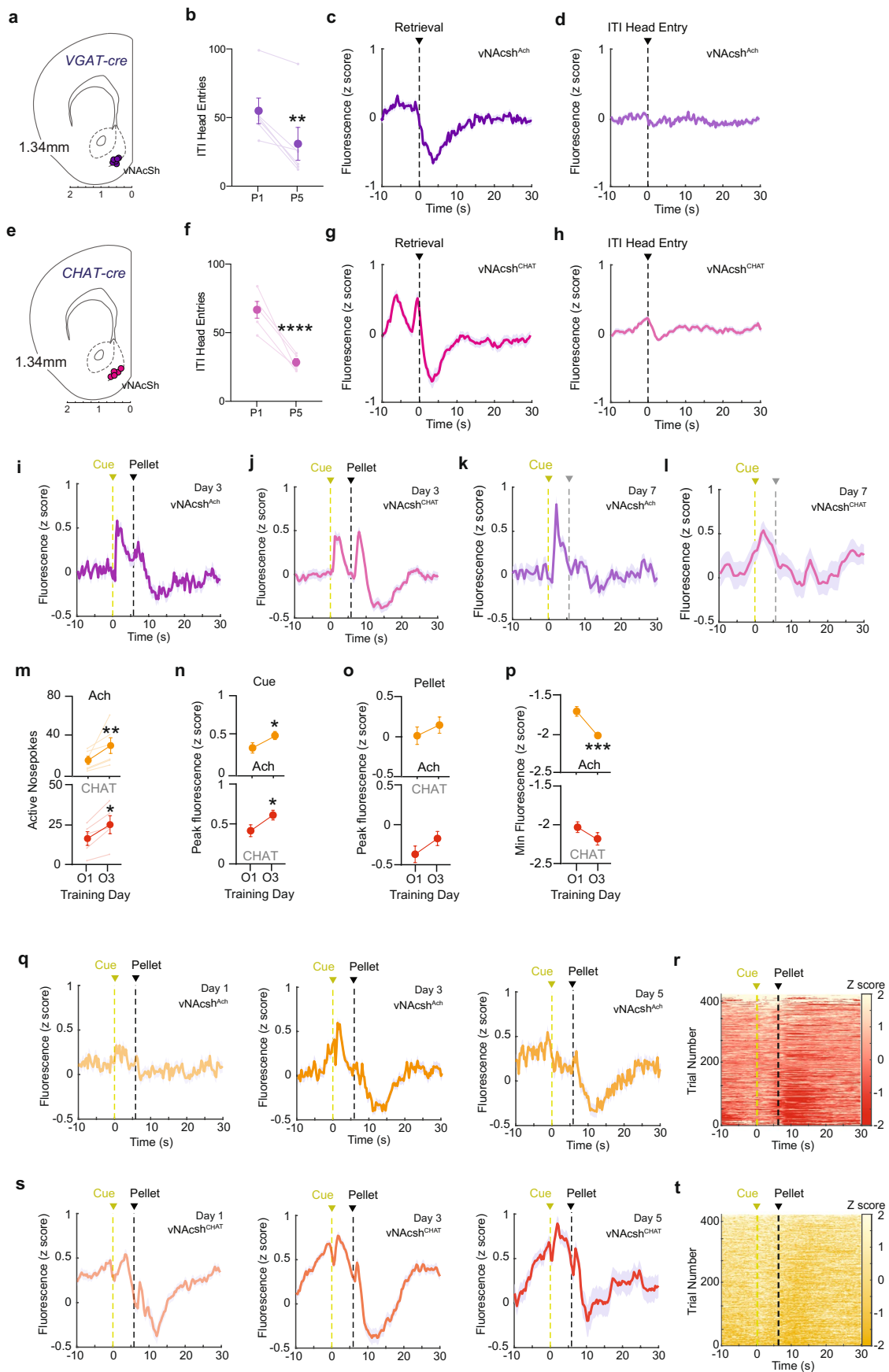
Extended Data Fig. 3 | See next page for caption.

Extended Data Fig. 3 | VTA GABAergic terminals project to and inhibit cholinergic interneurons in the NAc. (a) Top – Saggital brain cartoon depicting rostral-caudal position. Bottom – 20X confocal image of rostral VTA (left; -2.9 A/P relative to bregma, scalebar $-100 \mu\text{m}$), middle VTA (middle; -3.4 A/P relative to bregma, scalebar $-100 \mu\text{m}$) and caudal VTA (right; -3.8 A/P relative to bregma, scalebar $-100 \mu\text{m}$) showing expression of ChR2 (green) and DAPI (blue). (b) Table comparing electrophysiological parameters for CINs vs. MSNs – Rm: unpaired t-test: $t=3.000$, $p=0.0056$, $n=12$ (MSNs)–18(CINs), Cm: unpaired t-test: $t=0.3852$, $p=0.7030$, $n=12-18$, sIPSC frequency: unpaired t-test: $t=3.617$, $p=0.0040$, $n=8$ (CINs), 5(MSNs), sIPSC amplitude: unpaired t-test: $t=0.5700$, $p=0.5802$, $n=8,5$, Holding current: 2-way RM ANOVA, time x cell type interaction: $F_{1,18}=5.031$, $p=0.0377$; main effect of cell type: $F_{1,18}=28.29$, $p<0.0001$, post-hoc Sidak t-test – baseline vs. gabazine: CINs: $p=0.02$, MSNs: $p=0.8194$). Data represented as mean \pm SEM. (c) oIPSC amplitude comparing 5 Hz vs. 40 Hz stimulation (5 Hz: 269 ± 64 pA; 40 Hz: 280 ± 62 pA; paired t-test, $t=0.7367$, $p=0.4755$, $n=13$ cells/4 mice). Data represented as mean \pm SEM. (d) oIPSC area (nA^*s) over 250 ms period comparing 5 Hz vs. 40 Hz stimulation (5 Hz: 8 ± 3 nA^*s ; 40 Hz: 18 ± 4 nA^*s ; paired t-test, $t=3.804$, $p=0.0025$, $n=13$ cells/4 mice). Data represented as mean \pm SEM. (e) Image showing relative position of patch pipette for recordings in the vNAcSh. (f) Image showing relative position of patch pipette for recordings in the dNAcSh.



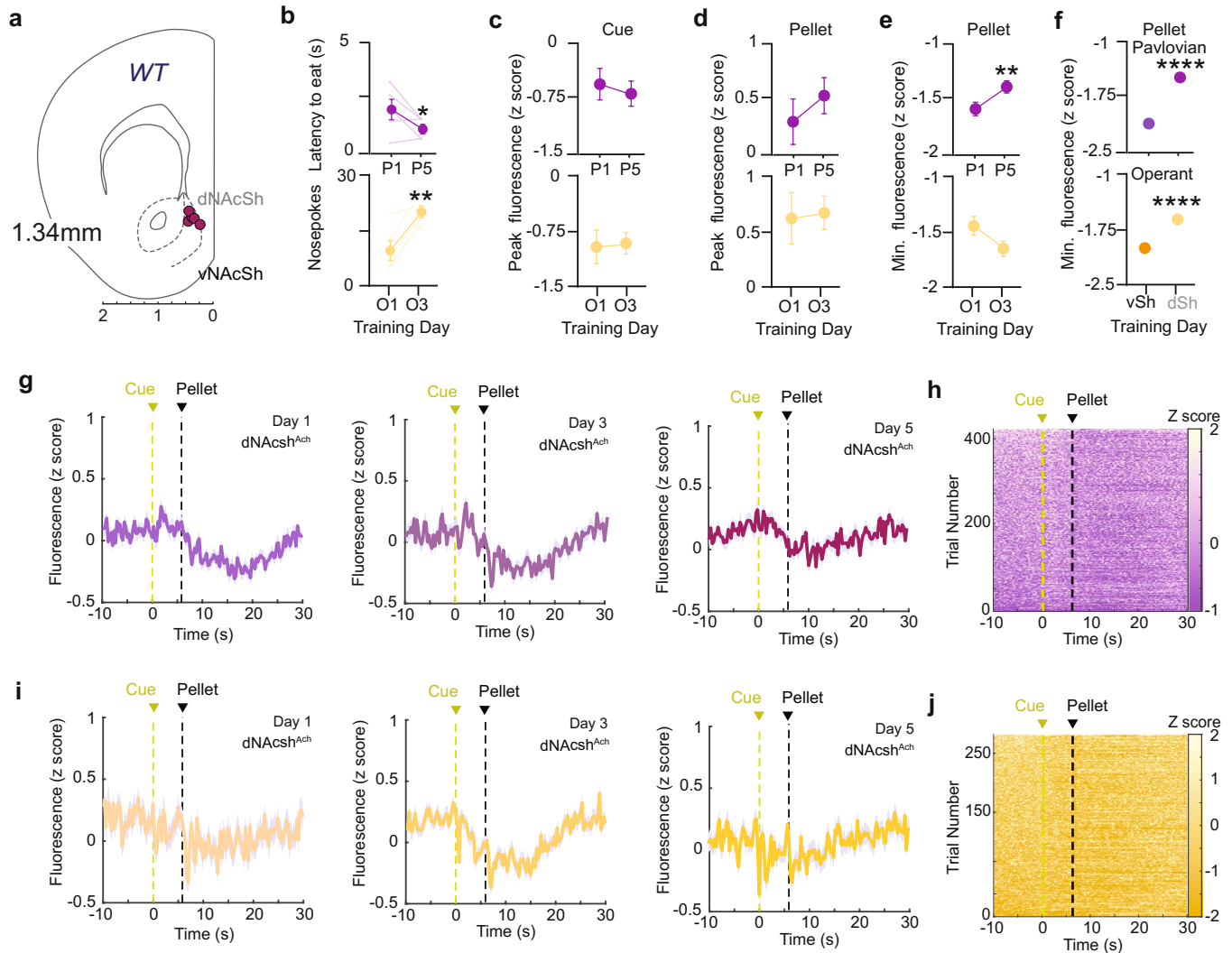
Extended Data Fig. 4 | See next page for caption.

Extended Data Fig. 4 | Photo-activation of vNAcSh cholinergic interneuron activity does not impact reinforcement. (a) Cartoon of ventral NAcSh virus and fiber optic placement. (b) Placement map showing fiber optic placements of each individual mouse included in the vNAcSh ChR2 group. (c) Data showing number of nose pokes during FR-1 self stimulation with no significant differences between control and experimental groups (data represented as mean \pm SEM, $n=7$ each, unpaired t test, $p=0.4165$, $t=0.8416$, $df=12$). (d) Cartoon of bilateral ventral NAcSh virus and fiber optic placement. (e) Representative examples of real-time mouse heatmap raster plots following no stimulation, 2 s phasic stimulation, and constant ventral NAcSh photostimulation. (f) Cartoon of bilateral ventral NAcSh virus and fiber optic placement. (g) No aversion real-time behavior following phasic photo-inhibition of ChAT neurons in ventral NAcSh (data represented as mean \pm SEM, $n=8$ mice/Control, 12 mice/Halo). (h) Total head entries performed in matched, counterbalanced sessions comparing laser on vs. off (pulse – 2 s on, 2 s ramp down, 1 s off). Left – ChR2 group ($n=9$ mice; Off vs. On paired t test $p=0.1328$, $t=1.673$, $df=8$). Right – YFP group ($n=6$ mice; Off vs. On paired t test $p=0.1629$, $t=1.635$, $df=5$). Data represented as mean \pm SEM.



Extended Data Fig. 5 | See next page for caption.

Extended Data Fig. 5 | Cholinergic interneuron activity and acetylcholine release in the vNACSh are inhibited during reward reinforcement. (a) Coronal brain cartoon of fiber placements in the vNACSh for VGAT-Cre+ mice injected with GRAB Ach3.0 (violet; $n=6$). (b) Inter-trial interval (ITI) head entries for Pavlovian training, vNACSh GRAB Ach3.0 ($n=6$ mice; P1 vs. P5 paired t test $p=0.0053$, $t=4.713$, $df=5$). (c) Mean vNACSh GRAB Ach3.0 recorded calcium activity during pellet retrieval averaged across all trials from day 1-5 of Pavlovian conditioning ($n=6$ mice). Data represented as mean \pm SEM. (d) Mean vNACSh GRAB Ach3.0 recorded calcium activity during unrewarded, ITI head entries averaged across all trials from day 1-5 of Pavlovian conditioning ($n=6$ mice). Data represented as mean \pm SEM. (e) Coronal brain cartoon of fiber placements in the vNACSh for CHAT-Cre+ mice injected with GCaMP6s (magenta; $n=5$). (f) Inter-trial interval (ITI) head entries for Pavlovian training, vNACSh GCaMP6s ($n=5$ mice; P1 vs. P5 paired t test $p=0.0034$, $t=6.20$, $df=4$). (g) Mean vNACSh GCaMP6s recorded calcium activity during pellet retrieval averaged across all trials from day 1-5 of Pavlovian conditioning ($n=5$ mice). Data represented as mean \pm SEM. (h) Mean vNACSh GCaMP6s recorded calcium activity during unrewarded, ITI head entries averaged across all trials from day 1-5 of Pavlovian conditioning ($n=5$ mice). Data represented as mean \pm SEM. (i) Mean vNACSh GRAB Ach3.0 recorded calcium activity averaged across all trials from day 3 of Pavlovian conditioning ($n=6$ mice). Data represented as mean \pm SEM. (j) Mean vNACSh GCaMP6s recorded calcium activity averaged across all trials from day 3 of Pavlovian conditioning ($n=5$ mice). (k) Mean vNACSh GRAB Ach3.0 recorded calcium activity averaged across all trials from day 7 of Pavlovian conditioning extinction ($n=6$ mice). (l) Mean vNACSh GCaMP6s recorded calcium activity averaged across all trials from day 7 of Pavlovian conditioning extinction ($n=5$ mice). (m) Top - vNACSh GRAB Ach3.0 active nosepekes for Operant training days ($n=6$ mice; O1 vs. O3 paired t test $p=0.0287$, $t=2.457$, $df=5$). Bottom - vNACSh GCaMP6s active nosepekes for Operant training days ($n=5$ mice; O1 vs. O3 paired t test $p=0.0129$, $t=4.274$, $df=4$). Data represented as mean \pm SEM. (n) Peak fluorescence during cue period (0-6 s) for Operant training days. Top - vNACSh GRAB Ach3.0 ($n=6$ mice; O1 vs. O3 paired t test $p=0.0364$, $t=1.810$, $df=263$). Bottom - vNACSh GCaMP6s ($n=5$ mice; O1 vs. O3 paired t test $p=0.0197$, $t=2.070$, $df=299$). Data represented as mean \pm SEM. (o) Peak fluorescence during reward period (6-30 s) for Operant training days. Top - vNACSh GRAB Ach3.0 ($n=6$ mice; O1 vs. O3 paired t test $p=0.1010$, $t=1.658$, $df=263$). Bottom - vNACSh GCaMP6s ($n=5$ mice; O1 vs. O3 paired t test $p=0.1423$, $t=1.471$, $df=299$). Data represented as mean \pm SEM. (p) Minimum fluorescence during reward period (6-30 s) for Operant training days. Top - vNACSh GRAB Ach3.0 ($n=6$ mice; O1 vs. O3 paired t test $p=0.0005$, $t=3.608$, $df=263$). Bottom - vNACSh GCaMP6s ($n=5$ mice; O1 vs. O3 paired t test $p=0.5695$, $t=0.5702$, $df=299$). Data represented as mean \pm SEM. (q) Mean vNACSh GRAB Ach3.0 recorded calcium activity averaged across all trials from day 1-5 of Operant conditioning ($n=6$ mice). Data represented as mean \pm SEM. (r) Heatmap raster plot of vNACSh GRAB Ach3.0 recorded calcium activity for every trial of Operant conditioning across all days. Trials are displayed in ascending order by average activity following pellet delivery ($n=7$ mice). (s) Mean vNACSh GCaMP6s recorded calcium activity averaged across all trials from day 1-5 of Operant conditioning ($n=5$ mice). Data represented as mean \pm SEM. (t) Heatmap raster plot of vNACSh GCaMP6s recorded calcium activity for every trial of Operant conditioning across all days. Trials are displayed in ascending order by average activity following pellet delivery ($n=5$ mice).



Extended Data Fig. 6 | Acetylcholine release in the dNAcSh is unchanged during reward reinforcement. (a) Coronal brain cartoon of fiber placements in the dNAcSh for WT mice injected with GRAB Ach3.0 (plum; $n=5$). (b) Top - dNAcSh GRAB Ach3.0 latency to eat for Pavlovian training days ($n=5$ mice; P1 vs. P5 paired t test $p=0.0284$, $t=2.654$, $df=4$). Bottom - dNAcSh GRAB Ach3.0 active nosepokes for Operant training days ($n=5$ mice; O1 vs. O3 paired t test $p=0.0057$, $t=5.395$, $df=4$). Data represented as mean \pm SEM. (c) Peak fluorescence during cue period (0-6 s) for Pavlovian or Operant training days. Top - dNAcSh GRAB Ach3.0 Pavlovian days ($n=5$ mice; P1 vs. P5 paired t test $p=0.6406$, $t=0.4683$, $df=95$). Bottom - dNAcSh GRAB Ach3.0 Operant days ($n=5$ mice; O1 vs. O3 paired t test $p=0.7091$, $t=0.3753$, $df=46$). Data represented as mean \pm SEM. (d) Peak fluorescence during reward period (6-30 s) for Pavlovian or Operant training days. Top - dNAcSh GRAB Ach3.0 Pavlovian days ($n=5$ mice; P1 vs. P5 paired t test $p=0.3495$, $t=0.9401$, $df=95$). Bottom - dNAcSh GRAB Ach3.0 Operant days ($n=5$ mice; O1 vs. O3 paired t test $p=0.3006$, $t=1.047$, $df=46$). Data represented as mean \pm SEM. (e) Minimum fluorescence during reward period (6-30 s) for Pavlovian or Operant training days. Top - dNAcSh GRAB Ach3.0 Pavlovian days ($n=5$ mice; P1 vs. P5 paired t test $p=0.0016$, $t=3.241$, $df=95$). Bottom - dNAcSh GRAB Ach3.0 Operant days ($n=5$ mice; O1 vs. O3 paired t test $p=0.7585$, $t=0.3093$, $df=46$). Data represented as mean \pm SEM. (f) Top - Minimum fluorescence during reward period (6-30 s) comparing vNAcsh ($n=6$ mice) vs. dNAcSh ($n=5$ mice) GRAB Ach3.0 for Pavlovian training (unpaired t test, $p<0.0001$, $t=9.760$, $df=422$). Bottom - Minimum fluorescence during reward period (6-30 s) comparing vNAcsh vs. dNAcSh GRAB Ach3.0 for Operant training (unpaired t test, $p<0.0001$, $t=5.470$, $df=278$). Data represented as mean \pm SEM. (g) Mean dNAcSh GRAB Ach3.0 recorded calcium activity averaged across all trials from day 1-5 of Pavlovian conditioning ($n=5$ mice). Data represented as mean \pm SEM. (h) Heatmap raster plot of dNAcSh GRAB Ach3.0 recorded calcium activity for every trial of Operant conditioning across all days. Trials are displayed in ascending order by average activity following pellet delivery ($n=5$ mice). (i) Mean dNAcSh GRAB Ach3.0 recorded calcium activity averaged across all trials from day 1-5 of Operant conditioning ($n=5$ mice). Data represented as mean \pm SEM. (j) Heatmap raster plot of dNAcSh GRAB Ach3.0 recorded calcium activity for every trial of Operant conditioning across all days. Trials are displayed in ascending order by average activity following pellet delivery ($n=5$ mice).

Reporting Summary

Nature Portfolio wishes to improve the reproducibility of the work that we publish. This form provides structure for consistency and transparency in reporting. For further information on Nature Portfolio policies, see our [Editorial Policies](#) and the [Editorial Policy Checklist](#).

Statistics

For all statistical analyses, confirm that the following items are present in the figure legend, table legend, main text, or Methods section.

n/a Confirmed

- The exact sample size (n) for each experimental group/condition, given as a discrete number and unit of measurement
- A statement on whether measurements were taken from distinct samples or whether the same sample was measured repeatedly
- The statistical test(s) used AND whether they are one- or two-sided
Only common tests should be described solely by name; describe more complex techniques in the Methods section.
- A description of all covariates tested
- A description of any assumptions or corrections, such as tests of normality and adjustment for multiple comparisons
- A full description of the statistical parameters including central tendency (e.g. means) or other basic estimates (e.g. regression coefficient) AND variation (e.g. standard deviation) or associated estimates of uncertainty (e.g. confidence intervals)
- For null hypothesis testing, the test statistic (e.g. F , t , r) with confidence intervals, effect sizes, degrees of freedom and P value noted
Give P values as exact values whenever suitable.
- For Bayesian analysis, information on the choice of priors and Markov chain Monte Carlo settings
- For hierarchical and complex designs, identification of the appropriate level for tests and full reporting of outcomes
- Estimates of effect sizes (e.g. Cohen's d , Pearson's r), indicating how they were calculated

Our web collection on [statistics for biologists](#) contains articles on many of the points above.

Software and code

Policy information about [availability of computer code](#)

Data collection For data collection, the following software was used : Ethovision XT, pClamp 11, MEDPC 5.

Data analysis For analysis, the following software was used: Prism 9, clampfit10, MATLAB R2020a. Custom MATLAB code used for data analysis is available at <https://github.com/BruchasLab>

For manuscripts utilizing custom algorithms or software that are central to the research but not yet described in published literature, software must be made available to editors and reviewers. We strongly encourage code deposition in a community repository (e.g. GitHub). See the Nature Portfolio [guidelines for submitting code & software](#) for further information.

Data

Policy information about [availability of data](#)

All manuscripts must include a [data availability statement](#). This statement should provide the following information, where applicable:

- Accession codes, unique identifiers, or web links for publicly available datasets
- A description of any restrictions on data availability
- For clinical datasets or third party data, please ensure that the statement adheres to our [policy](#)

All raw data will be made available upon request. A complete data availability statement is also provided in the manuscript.

Field-specific reporting

Please select the one below that is the best fit for your research. If you are not sure, read the appropriate sections before making your selection.

Life sciences Behavioural & social sciences Ecological, evolutionary & environmental sciences

For a reference copy of the document with all sections, see [nature.com/documents/nr-reporting-summary-flat.pdf](https://www.nature.com/documents/nr-reporting-summary-flat.pdf)

Life sciences study design

All studies must disclose on these points even when the disclosure is negative.

Sample size	Sample sizes were determined based on power analyses with a power value of 0.80 and an alpha value of 0.05.
Data exclusions	Exclusion criteria were pre-established. Exclusions were contingent only upon post-hoc validation of targeting for virus expression and fiber placements.
Replication	Experiments were replicated in at least two independent groups.
Randomization	Allocation of organisms and brain slices into experimental groups was done at random
Blinding	The experimenter was blinded to genotype/experimental group before and during all behavioral experiments.

Reporting for specific materials, systems and methods

We require information from authors about some types of materials, experimental systems and methods used in many studies. Here, indicate whether each material, system or method listed is relevant to your study. If you are not sure if a list item applies to your research, read the appropriate section before selecting a response.

Materials & experimental systems

Methods

n/a	Involved in the study	n/a	Involved in the study
<input type="checkbox"/>	<input type="checkbox"/> Antibodies	<input checked="" type="checkbox"/>	<input type="checkbox"/> ChIP-seq
<input checked="" type="checkbox"/>	<input type="checkbox"/> Eukaryotic cell lines	<input checked="" type="checkbox"/>	<input type="checkbox"/> Flow cytometry
<input checked="" type="checkbox"/>	<input type="checkbox"/> Palaeontology and archaeology	<input checked="" type="checkbox"/>	<input type="checkbox"/> MRI-based neuroimaging
<input type="checkbox"/>	<input checked="" type="checkbox"/> Animals and other organisms		
<input checked="" type="checkbox"/>	<input type="checkbox"/> Human research participants		
<input checked="" type="checkbox"/>	<input type="checkbox"/> Clinical data		
<input checked="" type="checkbox"/>	<input type="checkbox"/> Dual use research of concern		

Antibodies

Antibodies used	Anti-GFP (ab13970, Abcam, 1:2000 dilution) and Anti-Choline Acetyltransferase (ab144p, MilliporeSigma, 1:500 dilution)
Validation	All antibodies used included validation (published and commercial) by the vendor on the products' webpage. For Anti-GFP: https://www.abcam.com/gfp-antibody-ab13970.html https://pubmed.ncbi.nlm.nih.gov/32935839/ For Anti-ChAt: https://www.emdmillipore.com/US/en/product/Anti-Choline-Acetyltransferase-Antibody,MM_NF-AB144P#documentation https://pubmed.ncbi.nlm.nih.gov/25798106/

Animals and other organisms

Policy information about [studies involving animals](#); [ARRIVE guidelines](#) recommended for reporting animal research

Laboratory animals	Mice were group-housed, given access to food pellets and ad libitum, and maintained on a 12 hr:12 hr light:dark cycle (lights on at 7:00 AM). Humidity was maintained between 30-70%
Wild animals	No wild animals were used in the study
Field-collected samples	No field collected samples were used in this study
Ethics oversight	All the experiments were approved by the IACUC at the University of Washington at Seattle and Washington University at St. Louis

Note that full information on the approval of the study protocol must also be provided in the manuscript.